Contents

Introduction

This is a preliminary version, ***under work***, of the Lecture Notes of myself and Joachim Peinke, for the new module ***Advanced Fluid Mechanics - Transition to Turbulence & Turbulence - Applications to Transfers, Aerodynamics & Wind Energy*** at **Mines Nancy**, in the Departement Energy: Production, Transformation, at the Master 2 Level.

This module is somehow a follow up of the modules ***Mécanique des fluides*** (Plaut 2014) and ***Machines à fluides - Turbomachines*** (Jenny 2014) of the Master 1 Level. Indeed one can find, in the chapter 3 (resp. 6) of Plaut (2014), an introduction to Instabilities (resp. Turbulent flows); in the chapter 4 of Jenny (2014), an introduction to Wind Energy.

The aim of this document is to give a framework for the lectures, without details. The exercises will be most often solved during the lectures, and their solutions displayed in the 'Video presentations' that will be posted on the dynamic web page of the module[1]

http://emmanuelplaut.perso.univ-lorraine.fr/afm .

Accordingly, some equations here have some blank spaces, e.g., eq. (1.18). The student should write by himself the solutions here, after the lectures. A complete version of the document, without blank spaces, will be published after the final test.

We thank P. Milan for allowing us to reproduce a part of his Thesis in section 3.3.

Oldenburg & Nancy, January 24, 2015.

Joachim Peinke & Emmanuel Plaut.

[1]Please check this page for new versions of this document, and for the planning of this module.

Chapter 1

Rayleigh-Bénard Thermoconvection

This chapter corresponds to the Sessions 1 and 2 of 2014-2015. Note also that most of the material presented here is also presented with more details in Plaut (2008).

1.1 Generalities

Rayleigh-Bénard Thermoconvection (RBT; fig. 1.1) is a 'simple' closed fluid system, that permits well-controlled experiments, and may display complex Heat Transfer properties. In this system, contrarily to the case of a differentially heated cavity studied by Davis (1983), thermoconvection can only come in through an ***instability*** of the conduction state.

We assume the ***Boussinesq approximation***, that states that the density ρ of the fluid depends on its temperature T according to

$$\rho \;=\; \rho_0\,[1-\alpha(T-T_0)] \tag{1.1}$$

with ρ_0 the reference density, T_0 the reference temperature, α the thermal expansion coefficient. Consequently the Boussinesq equations for the velocity field $\overline{\mathbf{v}}$, the pressure field p and the temperature field T read

$$\mathrm{div}\overline{\mathbf{v}} \;=\; 0\;, \tag{1.2}$$

$$\frac{d\overline{\mathbf{v}}}{dt} \;=\; -\,\alpha T\,\overline{\mathbf{g}} \;-\; \overline{\boldsymbol{\nabla}}p' \;+\; \nu\overline{\boldsymbol{\Delta}}\overline{\mathbf{v}}\;, \tag{1.3}$$

$$\frac{dT}{dt} \;=\; \kappa\Delta T\;. \tag{1.4}$$

Here $\overline{\mathbf{g}}$ is the acceleration due to gravity, ν the kinematic viscosity of the fluid, κ its heat diffusivity. The pressure is a modified one, hence the notation p'.
These equations always admit a static solution that satisfies the isothermal boundary conditions:

$$\overline{\mathbf{v}} \;=\; \overline{\mathbf{0}}\;,\quad T \;=\; T_0 \;-\; \delta T\frac{z}{d}\quad\text{with}\quad \delta T \;=\; T_2-T_1\;.$$

This proves that convection can only set in through an ***instability*** of this static solution.
We introduce dimensionless equations with the thickness d as the unit of length, the heat diffusion time

$$\tau_{\mathrm{therm}} \;=\; d^2/\kappa$$

as the unit of time,

$$V \;=\; d/\tau_{\mathrm{therm}} \;=\; \kappa/d$$

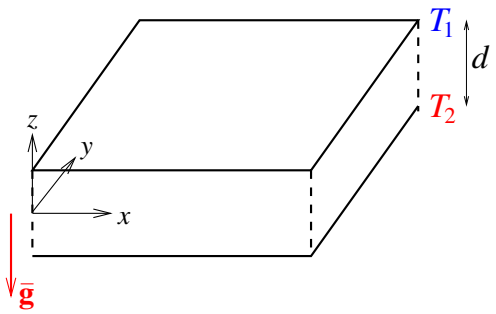

Fig. 1.1 : The ***Rayleigh-Bénard Thermoconvection*** system. A layer of fluid is sandwiched between two horizontal, isothermal plates, with $T_2 > T_1$.

as the unit of velocity, δT as the unit of temperature. We also introduce a dimensionless perturbation of temperature θ, such that the dimensionless temperature

$$T' \;=\; T'_0 \;-\; z' \;+\; \theta$$

Dropping the primes for the dimensionless quantities, we get the ***dimensionless Boussinesq equations***

$$\mathrm{div}\overline{\mathbf{v}} \;=\; 0 \;, \tag{1.5}$$

$$P^{-1}\frac{d\overline{\mathbf{v}}}{dt} \;=\; R\theta\,\overline{\mathbf{e}}_z \;-\; \overline{\boldsymbol{\nabla}}p \;+\; \overline{\boldsymbol{\Delta}}\overline{\mathbf{v}} \;, \tag{1.6}$$

$$\frac{d\theta}{dt} \;=\; \Delta\theta \;+\; v_z \;, \tag{1.7}$$

with

$$\text{the } \textbf{\textit{Rayleigh number}} \;\; R \;=\; \alpha\delta T g d^3/(\kappa\nu) \quad \text{and} \quad \text{the } \textbf{\textit{Prandtl number}} \;\; P \;=\; \nu/\kappa \;. \tag{1.8}$$

Because of the ***isotropy of the problem in the horizontal plane*** we may focus on 2D xz solutions

$$\overline{\mathbf{v}} \;=\; v_x(x,z,t)\,\overline{\mathbf{e}}_x \;+\; v_z(x,z,t)\,\overline{\mathbf{e}}_z \;, \quad \theta \;=\; \theta(x,z,t) \;. \tag{1.9}$$

Thus the mass-conservation equation (1.5) can be solved conveniently by using a ***streamfunction*** ψ such that

$$\overline{\mathbf{v}} \;=\; \overline{\mathbf{curl}}(\psi\,\overline{\mathbf{e}}_y) \;=\; -\,(\partial_z\psi)\,\overline{\mathbf{e}}_x \;+\; (\partial_x\psi)\,\overline{\mathbf{e}}_z \;. \tag{1.10}$$

Moreover, the pressure can be eliminated by solving, instead of the Navier-Stokes equation (1.6), the vorticity equation, which reduces to its component in the y direction,

$$P^{-1}\partial_t(-\Delta\psi) \;+\; P^{-1}\big[\partial_z\big(\overline{\mathbf{v}}\cdot\overline{\boldsymbol{\nabla}}v_x\big) - \partial_x\big(\overline{\mathbf{v}}\cdot\overline{\boldsymbol{\nabla}}v_z\big)\big] \;=\; -\,R\partial_x\theta \;+\; \Delta(-\Delta\psi) \;. \tag{1.11}$$

To put the equations (1.11) and (1.7) under a 'matrix form', we introduce the ***local state vector***

$$V \;=\; (\psi,\theta) \;. \tag{1.12}$$

It fulfills

$$\boxed{D\cdot\partial_t V \;=\; L_R\cdot V \;+\; N_2(V,V)} \tag{1.13}$$

$$\text{with} \qquad [D\cdot\partial_t V]_1 \;=\; P^{-1}(-\Delta\partial_t\psi) \;, \quad [L_R\cdot V]_1 \;=\; -\,R\partial_x\theta \;+\; \Delta(-\Delta\psi) \;, \tag{1.14a}$$

$$[N_2(V,V)]_1 \;=\; P^{-1}\big[\partial_z\big(\overline{\mathbf{v}}\cdot\overline{\boldsymbol{\nabla}}v_x\big) - \partial_x\big(\overline{\mathbf{v}}\cdot\overline{\boldsymbol{\nabla}}v_z\big)\big] \;, \tag{1.14b}$$

$$[D\cdot\partial_t V]_2 \;=\; \partial_t\theta \;, \quad [L_R\cdot V]_2 \;=\; \Delta\theta \;+\; v_z \;, \quad [N_2(V,V)]_2 \;=\; -\,\overline{\mathbf{v}}\cdot\overline{\boldsymbol{\nabla}}\theta \;. \tag{1.14c}$$

The boundary conditions on θ describe isothermal boundaries:

$$\theta = 0 \quad \text{if} \quad z = \pm 1/2 \ . \tag{1.15}$$

The boundary conditions on ψ describe slip boundaries without shear stress,

$$v_z = 0 \quad \text{and} \quad \partial_z v_x = 0 \quad \Longleftrightarrow \quad \partial_x \psi = \partial_z^2 \psi = 0 \quad \text{if} \quad z = \pm 1/2 \ , \tag{1.16}$$

or no-slip boundaries

$$v_x = v_z = 0 \quad \Longleftrightarrow \quad \partial_x \psi = \partial_z \psi = 0 \quad \text{if} \quad z = \pm 1/2 \ . \tag{1.17}$$

1.2 Linear stability analysis of slip RBT

This analysis allows one to identify a ***critical Rayleigh number***

$$R_c \ = \tag{1.18}$$

above which a first normal mode, solution of

$$\sigma D \cdot V_1(\mathbf{q}) \ = \ L_R \cdot V_1(\mathbf{q}) \ , \tag{1.19}$$

with σ the temporal eigenvalue, becomes amplified. This ***critical mode*** has an x-wavenumber which is the ***critical wavenumber***

$$k_c \ = \qquad\qquad . \tag{1.20}$$

Thus ***'roll patterns'***, with periodic modulations of the average temperature, appear spontaneously just above onset, with the ***critical wavelength***

$$\lambda_c \ = \ 2\pi/k_c \ = \qquad\qquad . \tag{1.21}$$

This corresponds to a ***patterning bifurcation***. This is confirmed by experiments, such as the ones of Hu *et al.* (1993), which display nice roll patterns.

Exercise 1.1 ***General linear stability analysis of slip RBT***

To perform a general linear stability analysis of the problem (1.13) with the boundary conditions (1.15) and (1.16), it is more convenient to use another frame $Oxyz'$ where the layer is located between $z' = 0$ (bottom plate) and $z' = 1$ (top plate), i.e., to use $z' = z + 1/2$. In this Exercise, we note z instead of z', i.e. $z \in \ ]0{,}1[$.

1 Calculate ***systematically*** all x-homogeneous normal modes, that do not depend on x, and have been disregarded during the lecture. Show that they are indeed 'irrelevant'.

Indications:

Observe that the heat and vorticity equations are decoupled.
First, solve the heat equation. Search solutions of the form $\theta = a_+ \ e^{rz} + a_- \ e^{-rz}$. Establish a link between r and the temporal eigenvalue σ. With the boundary conditions, obtain an homogeneous system on (a_+,a_-). Explain why the determinant of this system must vanish. From this condition, obtain the values of σ and finally the form of θ.
Second, observe that ψ'' obeys an equation similar to the heat equation...

2 Focus now on x-dependent solutions. During the lecture, we have calculated only one family of Fourier normal modes,

$$V_1(k,\pm) \;=\; (\Psi(k,\pm),\, \Theta(k,\pm))\;\exp(ikx)\;\sin(\pi z)\;, \tag{1.22}$$

with $k \neq 0$ the x-wavenumber. Thus, the fact that an initial condition

$$V(t=0) \;=\; (\psi(t=0),\, \theta(t=0))$$

can be decomposed on the basis of all normal modes

$$V(t=0) \;=\; \sum_{\mathbf{q}} A(\mathbf{q}) V_1(\mathbf{q})$$

is unclear, as is also the precise meaning of $\mathbf{q}$, the labels that index all normal modes.
For the sake of simplicity, we consider periodic boundary conditions in the x direction, under $x \mapsto x + L$. Hence exponential Fourier series can be used to analyse the x dependence, i.e. $\mathbf{q}$ contains generally the x-wavenumber k such that

$$V_1(\mathbf{q}) \;=\; V_1(k,\mathbf{q}') \;=\; V_1(z;k,\mathbf{q}')\;\exp(ikx)$$

with $k \in \mathbb{K}$, $\mathbb{K} = (2\pi/L)\mathbb{Z}$, $\mathbf{q}'$ other labels that have to be identified.

Show that modes

$$V_1(k,\pm,n) \;=\; (\Psi(k,\pm,n),\, \Theta(k,\pm,n))\;\exp(ikx)\;\sin(n\pi z)$$

with $n \in \mathbb{N}^*$ are also normal modes, and establish a characteristic equation for the temporal eigenvalue σ. Check that for given k and n, there are indeed two modes $+$ and $-$ and two eigenvalues $\sigma(k,\pm,n)$. Check that with $n = 1$ you recover the modes (1.22) and their corresponding eigenvalues. Check that the most relevant modes are indeed the modes with $n = 1$.

Comments:

From a mathematical point of view, the fact that any initial condition can be written as

$$V(t=0) \;=\; \sum_{k\in\mathbb{K}} \sum_{s=\pm} \sum_{n\in\mathbb{N}^*} A(k,s,n)\; V_1(k,s,n)$$

results from a development in exponential Fourier series of x, trigonometric Fourier series of z, and from the fact that, for given k and n, $(\Psi(k,+,n),\, \Theta(k,+,n))$ and $(\Psi(k,-,n),\, \Theta(k,-,n))$ form a basis of $\mathbb{C}^2$.
Coming back to $z \in\,]-1/2,1/2[$, the following symmetry property can be shown all normal modes are *either* even *or* odd under the midplane reflection symmetry $z \mapsto -z$.

1.3 The linear modes basis - The adjoint problem - adjoint modes

Hereafter we work in a box with periodic boundary conditions under $x \mapsto x + \lambda_c$. Consequently the wavenumber $k \in \mathbb{K}$ with $\mathbb{K} = k_c\mathbb{Z}$. Hence we can label the normal modes with $\mathbf{q} = (k,s,n) \in \mathbb{K} \times \{+,-\} \times \mathbb{N}^*$, and a general field can always be written as a superposition of normal modes,

$$V \;=\; \sum_{k\in\mathbb{K}} \sum_{s=\pm} \sum_{n\in\mathbb{N}^*} A(k,s,n)\; V_1(k,s,n) = \;\sum_{\mathbf{q}} A(\mathbf{q})\; V_1(\mathbf{q})\;. \tag{1.23}$$

It is important to be able to calculate systematically the 'amplitudes' $A(\mathbf{q})$. For this purpose, we introduce (generally, the technique is not only specific to RBT) the ***adjoint problem*** and ***adjoint modes*** as follows.

- We first introduce the ***Hermitian inner product***

$$\langle V,U\rangle \;=\; \int_{x=0}^{\lambda_c}\int_{z=-1/2}^{1/2} V(x,z)\cdot U^*(x,z)\;\frac{dx}{\lambda_c}\;dz\;. \tag{1.24}$$

- We then define the ***adjoint operators*** $D^\dagger$ and $L^\dagger$ such that

$$\forall V,U,\quad \langle D\cdot V,U\rangle \;=\; \Big\langle V,D^\dagger\cdot U\Big\rangle \quad\text{and}\quad \langle L\cdot V,U\rangle \;=\; \Big\langle V,L^\dagger\cdot U\Big\rangle\;, \tag{1.25}$$

  V and U satisfying the boundary conditions of the problem.

- We assume[1] that the ***adjoint eigenproblem***

$$\sigma^* D^\dagger\cdot U \;=\; L^\dagger\cdot U \tag{1.26}$$

  has eigenvalues that are the complex conjugates of the ones of the direct eigenproblem.

- Therefore to each direct mode $V_1(\mathbf{q})$ of eigenvalue $\sigma(\mathbf{q})$ there correspond ***adjoint modes*** $U_1(\mathbf{q})$ of eigenvalue $\sigma^*(\mathbf{q})$ with the same wavenumber k.

- If k in $\mathbf{q}\;\neq k'$ in $\mathbf{q}'$ then

$$\big\langle D\cdot V_1(\mathbf{q}),U_1(\mathbf{q}')\big\rangle \;=\; \big\langle L\cdot V_1(\mathbf{q}),U_1(\mathbf{q}')\big\rangle \;=\; 0\;. \tag{1.27}$$

- For $\mathbf{q}$ with the same wavenumber k, one has usually non degenerate eigenvalues:

$$\text{if } k \text{ in } \mathbf{q} \;=\; k \text{ in } \mathbf{q}' \;\text{ but }\; \mathbf{q}\neq\mathbf{q}'\;,\quad \sigma=\sigma(\mathbf{q}) \;\neq\; \sigma'=\sigma(\mathbf{q}')\;. \tag{1.28}$$

- Consequently one can show that

$$\mathbf{q}\neq\mathbf{q}' \quad\Longrightarrow\quad \big\langle D\cdot V_1(\mathbf{q}),U_1(\mathbf{q}')\big\rangle \;=\; \big\langle L\cdot V_1(\mathbf{q}),U_1(\mathbf{q}')\big\rangle \;=\; 0\;. \tag{1.29}$$

- Normalizing the adjoint modes such that

$$\forall\mathbf{q}\;,\quad \langle D\cdot V_1(\mathbf{q}),U_1(\mathbf{q})\rangle \;=\; 1\;, \tag{1.30}$$

  we find that the amplitudes in (1.23) are given by

$$\boxed{A(\mathbf{q}) \;=\; \langle D\cdot V,U_1(\mathbf{q})\rangle}\;. \tag{1.31}$$

[1] This is very often the case, at least this works for RBT.

Exercise 1.2 ***Adjoint problem in slip RBT***

Denoting $U = (\psi_a, \theta_a)$, calculate analytically the adjoint problem of the RBT linearized problem, with slip boundaries. Focus on the case of Fourier modes in x, of x-wavenumber $k = mk_c$ with $m \in \mathbb{Z}^*$.

Indications:

Start with the calculation of $D^\dagger$. It will be useful to use ***recursive integrations by parts***: if u and v are functions of z of class C^n, one has

$$\int uv^{(n)}\, dz \;=\; \Big[uv^{(n-1)} \;-\; u'v^{(n-2)} \;+\; u''v^{(n-3)} \;+\; \ldots \;+\; (-1)^{n-1}u^{(n-1)}v\Big] \;+\; (-1)^n \int u^{(n)}v\, dz$$

which can be explicited with the help of this table:

	Column A Derivatives of u	Column B Derivatives of v
$+$	u	$v^{(n)}$
$-$	$u^{(1)}$	$v^{(n-1)}$
	$\vdots$	$\vdots$
$(-1)^n$	$u^{(n)}$	v

and of this rule: pair the 1st entry of column A with the 2nd entry of column B, the 2nd entry of column A with the 3rd entry of column B, etc... with alternating signs (beginning with the positive sign)...

Solution:

$$D^\dagger \;=\; \quad , \quad [L_R^\dagger \cdot U]_1 \;=\; \quad , \quad [L_R^\dagger \cdot U]_2 \;=\; \quad . \tag{1.32}$$

Exercise 1.3 ***Adjoint critical mode in RBT with slip boundaries***

For $k = k_c = \pi/\sqrt{2}$, $R \;=\; R_c \;=\; 27\pi^4/4$, to the critical mode

$$V_{1c} \;=\; (-3i\pi/\sqrt{2},\, 1)\; \exp(ik_c x)\; \cos(\pi z)\;, \tag{1.33}$$

check that there corresponds a neutral adjoint critical mode U_{1c}, and calculate it with the normalization condition (1.30).

Solution:

$$U_{1c} \;=\; \quad . \tag{1.34}$$

1.4 Weakly Nonlinear Analysis of slip RBT

We seek, for R close to R_c or

$$\epsilon \;=\; R/R_c - 1 \;\ll\; 1\;, \tag{1.35}$$

which is denoted as the 'bifurcation parameter', an approximate solution of the nonlinear problem (1.13) of the form (1.23),

$$V \;=\; \sum_{\mathbf{q}} A(\mathbf{q},t)\; V_1(\mathbf{q})\;. \tag{1.36}$$

Following Haken (1983) *'Long-living systems slave short-living systems'*, we distinguish

- ***active modes*** $\mathbf{q} = \mathbf{q}_c = (k_c, +, 1)$ or $\mathbf{q}_c^* = (-k_c, +, 1)$ which are long-living

$$\sigma(\mathbf{q}, R) \sim \epsilon/\tau_0 \tag{1.37}$$

  with

$$\tau_0 = \tag{1.38}$$

  the characteristic time of the instability,

- from the ***passive modes*** $\mathbf{q} \neq \mathbf{q}_c, \mathbf{q}_c^*$ which are short-living (rapidly damped)

$$\sigma(\mathbf{q}, R) < \sigma_1 < 0 \, . \tag{1.39}$$

We assume that, possibly after a short transient, the active modes dictate the dynamics:

$$\forall \mathbf{q} \, , \quad \frac{dA}{dt}(\mathbf{q}, t) = O(\epsilon \, A(\mathbf{q}, t)) \, , \tag{1.40}$$

$$V = V_a + V_\perp \quad \text{with} \quad V_a = A_{1c} V_{1c} + c.c. \text{ the } \textbf{active modes}, V_a \ll 1 \, , \tag{1.41}$$

$$V_\perp = \sum_{\mathbf{q} \neq \mathbf{q}_c, \mathbf{q}_c^*} A(\mathbf{q}, t) \, V_1(\mathbf{q}) \text{ the } \textbf{passive modes}, V_\perp \ll V_a \, . \tag{1.42}$$

In the amplitude equations for the passive modes,

$$\frac{dA}{dt}(\mathbf{q}, t) = \sigma(\mathbf{q}, R) A(\mathbf{q}, t) + \sum_{\mathbf{q}_1} \sum_{\mathbf{q}_2} A(\mathbf{q}_1, t) A(\mathbf{q}_2, t) \, \langle N_2(V_1(\mathbf{q}_1), V_1(\mathbf{q}_2)), U_1(\mathbf{q}) \rangle \, , \tag{1.43}$$

we may neglect dA/dt and consider that these modes are created by the active ones, through nonlinear effects. The passive modes are therefore obtained by ***quasistatic elimination***

$$0 = \sigma(\mathbf{q}, R) A(\mathbf{q}, t) + \sum_{\mathbf{q}_1 = \mathbf{q}_c, \mathbf{q}_c^*} \sum_{\mathbf{q}_2 = \mathbf{q}_c, \mathbf{q}_c^*} A(\mathbf{q}_1, t) A(\mathbf{q}_2, t) \, \langle N_2(V_1(\mathbf{q}_1), V_1(\mathbf{q}_2)), U_1(\mathbf{q}) \rangle \tag{1.44}$$

which amounts here, for 'symmetry' reasons[2], to

$$0 = L_R \cdot V_\perp + N_2(V_a, V_a) \, . \tag{1.45}$$

Exercise 1.4 ***Quasistatic elimination of the passive modes in slip RBT***

In slip RBT, denoting $A = A_{1c}$ the amplitude of the critical mode, show with Mathematica that

$$[N_2(V_a, V_a)]_1 = 0 \, , \quad [N_2(V_a, V_a)]_2 = B \, \sin(2\pi z) \tag{1.46}$$

with B a real number,

$$B = \qquad . \tag{1.47}$$

Next, solve (1.45), showing that

$$V_\perp = A^2 V_{20} \quad \text{with} \quad V_{20} = \qquad , \tag{1.48}$$

and explain the physics behind.

[2] The nonlinear terms $N_2(V_a, V_a)$ create only passive modes, of x-wavenumber 0 or $\pm 2k_c$ which are quite different from k_c.

Exercise 1.5 ***Passive modes in slip RBT first control the Nusselt number***

Show that the passive mode that you have calculated controls the value of the Nusselt number

$$\mathrm{Nu} \;=\; \frac{\Phi_{\text{heat with conduction \& convection}}}{\Phi_{\text{heat with conduction only}}} \tag{1.49}$$

with Φ_{heat} the average heat flux that goes from the hot bottom plate to the cold top plate.

Indication: you must prove that $\mathrm{Nu}-1 \propto A^2$.

Solution:

$$\mathrm{Nu}-1 \;=\; \qquad . \tag{1.50}$$

To determine A, we obtain, by projection of (1.13) onto the adjoint critical mode U_{1c}, the ***amplitude equation***

$$\frac{dA}{dt} \;=\; \frac{\epsilon}{\tau_0}A \;+\; \langle N_2(V,V),U_{1c}\rangle \;. \tag{1.51}$$

The nonlinear terms in $N_2(V,V)$ that have a nonzero projection on $U_1(\mathbf{q}_c)$ are ***'resonant'***.

Exercise 1.6 ***Resonant terms in slip RBT at order*** A^3

Compute with Mathematica the resonant terms in $N_2(V,V)$, and explain their physics.

Solution:

$$[N_2(V,V)\text{ resonant}]_1 \;=\; \quad,\quad [N_2(V,V)\text{ resonant}]_2 \;=\; \qquad . \tag{1.52}$$

Exercise 1.7 ***Saturation in slip RBT***

Show that $\langle N_2(V,V),U_{1c}\rangle = -gA^3$ and compute the ***saturation coefficient***

$$g \;=\; \qquad . \tag{1.53}$$

Deduce from this and the knowledge of τ_0 an analytical expression of the Nusselt number in weakly nonlinear roll solutions,

$$\mathrm{Nu} \;=\; \qquad . \tag{1.54}$$

Comment: consequently $\mathrm{Nu}-1 \propto \delta T/(\delta T)_c - 1$, with $(\delta T)_c$ the critical value of the temperature difference; this is confirmed by experiments, see e.g. the fig. 4 of Hu *et al.* (1993).

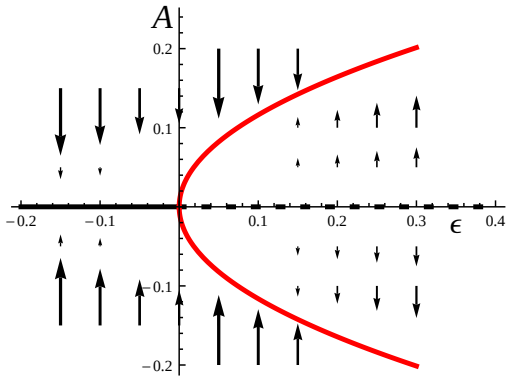

Fig. 1.2 : Stationary solutions, or 'fixed points', of the amplitude equation (1.55). With the continuous lines: stable solutions; with the dashed line: unstable solution. The arrows show vectors $(0,\, dA/dt)$ when $A(t)$ evolves according to eq. (1.55), from an initial condition which is not a fixed point.

In conclusion, the ***amplitude equation*** (1.51) assumes the form

$$\boxed{\frac{dA}{dt} \;=\; \frac{\epsilon}{\tau_0} A \;-\; g A^3} \qquad \text{with} \qquad g \in \mathbb{R}^{+*} \;. \tag{1.55}$$

This is the generic equation of a ***supercritical pitchfork bifurcation***. It is easy to calculate the stationary solutions, or 'fixed points', of eq. (1.55):

$$\begin{aligned} \forall \epsilon \quad &, \quad A \;=\; 0 \;, \\ \forall \epsilon > 0 \quad &, \quad A \;= \qquad\qquad\quad , \end{aligned} \tag{1.56}$$

and to construct a diagram in the plane (ϵ, A) (bifurcation parameter, amplitude) plotting these solutions, that depend on ϵ, and arrows parallel to the A-axis indicating dA/dt. From the direction of these arrows, the trajectories of the dynamical system (1.55), which are line segments, can be immediately deduced. From this, the stability properties of the stationary solutions ensue... The result is shown in fig. 1.2, which displays a *'pitchfork'*; moreover, the interesting non-vanishing stationary solutions exist only for $\epsilon > 0$ i.e. *above* (*'super'* in latin) onset; all this explain the name of the bifurcation...

1.5 Numerical Linear Analysis of no-slip RBT

Exercise 1.8 ***Numerical linear stability analysis of no-slip RBT with a spectral method***

To solve with Mathematica the linear RBT problem using no-slip boundary conditions, for $P = 1$, use a ***spectral expansion*** of the eigenfunctions of the Fourier modes, in $\exp(ikx)$, as a sum of simple polynomial functions that fulfill the boundary conditions:

$$\Psi(z) \;=\; \sum_{n=1}^{N} \Psi_n F_n(z) \qquad \text{with} \qquad F_n(z) \;=\; (1/2 - z)^2 \, (z + 1/2)^2 \, T_{2n-2}(2z) \;, \tag{1.57}$$

$$\Theta(z) \;=\; \sum_{n=1}^{N} \Theta_n f_n(z) \qquad \text{with} \qquad f_n(z) \;=\; (1/2 - z) \, (z + 1/2) \, T_{2n-2}(2z) \;, \tag{1.58}$$

T_n the n^{th} Chebyshev polynomial of the first kind, N the number of z-modes.

1 Plot a few functions F_n and f_n, and the ***Gauss-Lobatto collocation points***

$$z_m \;=\; \cos[m\pi/(2N+1)]/2 \quad \text{for} \quad m \in \{1,2,\cdots,N\}\;, \tag{1.59}$$

and comment.

2 By evaluating the vorticity and heat equation at the Gauss-Lobatto collocation points, construct by blocks matrices that represent the operators D and L_R applied to the vector of the expansion coefficients $V_{\rm num} = (\Psi_1,\cdots,\Psi_N,\Theta_1,\cdots,\Theta_N)$. Note that n in equations (1.57) and (1.58) is a 'column index', m in equation (1.59) is a 'line index'.

3 With the command `Eigenvalues`, find a numerical approximation of the temporal eigenvalues $\sigma(k,R)$ for k fixed. Check the physical relevance of this 'spectrum'.

4 Sort these eigenvalues to find the most relevant one $\sigma_1(k,R)$.

5 Define the neutral Rayleigh number $R_0(k)$ by finding a root of $\sigma_1(k,R) = 0$.

6 Finally, find the critical parameters by minimizing the neutral Rayleigh number.
Compare with the slip case and discuss the physics.

1.6 Very short review of no-slip RBT

The numerical method described in Exercise 1.8 can be extended to perform a weakly nonlinear analysis of no-slip RBT. An highly nonlinear analysis can also be performed to compute roll solutions far from onset, and the numerical results agree well with the experiments at large Prandtl number of Stasiek (1997). However, especially at small Prandtl numbers, nonlinear rolls become quickly unstable when the Rayleigh number increases, as shown for instance in Plapp (1997); Bodenschatz *et al.* (2000). These secondary instabilities have been studied in great details by Busse and coworkers (Busse 2003). After tertiary instabilities, etc... this leads at high Rayleigh numbers to ***turbulent flows***. These scenarios of a ***progressive transition to turbulence through a cascade of instabilities*** can be coined as ***'globally supercritical'***.

Chapter 2

Transition to Turbulence in Open Shear Flows

*This chapter (**under work** !) corresponds to the Sessions 6 and 7 of 2014-2015, but from a pedagogical point of view it is presented here, before we dive into fully turbulent flows.*

2.1 Generalities

Open Shear Flows are often encountered in Aerodynamics, think for instance to the Flow around an Airfoil, and also in Hydrodynamics, think for instance to Pipe Flow or Channel Flow.

For the sake of simplicity, we focus here on ***2D xz Flows***, such as the Boundary Layer Flow over a flat plate (fig. 2.1a) or Flows in channels (fig. 2.1b). It is assumed that in the y direction, the boundaries of the system are far away and have a little influence. Not too close to the leading edge, the Boundary Layer over a flat plate (fig. 2.1a) is quasi invariant under translations in the x direction. To simplify, we will consider hereafter ***Parallel Open Shear Flows*** that are strictly invariant under translations in the x direction. They are generally of the form

$$\overline{\mathbf{v}} \;=\; \overline{\mathbf{v}}_0 \;=\; U(z)\,\overline{\mathbf{e}}_x\;,\quad \widehat{p} \;=\; p+\rho g Z \;=\; \widehat{p}_0 \;=\; -\,Gx\;, \tag{2.1}$$

with Z the vertical coordinate, G the pressure gradient necessary to sustain the Flow if the fluid is viscous. If the fluid is inviscid, $G=0$.
We want to analyze the ***stability*** of such basic Flows.
For this purpose, we introduce ***perturbations*** of velocity and pressure, i.e., we write

$$\overline{\mathbf{v}} \;=\; \overline{\mathbf{v}}_0 \;+\; \overline{\mathbf{u}}\;,\quad \widehat{p} \;=\; \widehat{p}_0 \;+\; p'\;. \tag{2.2}$$

The Navier-Stokes or Euler equation then give

$$\partial_t\overline{\mathbf{u}} \;+\; U'u_z\overline{\mathbf{e}}_x \;+\; U\partial_x\overline{\mathbf{u}} \;+\; (\overline{\mathbf{u}}\cdot\overline{\boldsymbol{\nabla}})\overline{\mathbf{u}} \;=\; -\,(1/\rho)\overline{\boldsymbol{\nabla}}p' \;+\; \nu\overline{\boldsymbol{\Delta}}\overline{\mathbf{u}}\;. \tag{2.3}$$

Moreover, we assume that the fluid is incompressible,

$$\mathrm{div}\overline{\mathbf{u}} \;=\; 0\;. \tag{2.4}$$

We introduce dimensionless equations using a length scale h which is the thickness of the mixing layer, the half-width of the channel, ... For the velocity scale, we use

$$U_0 \;=\; \max_z U(z)\;. \tag{2.5}$$

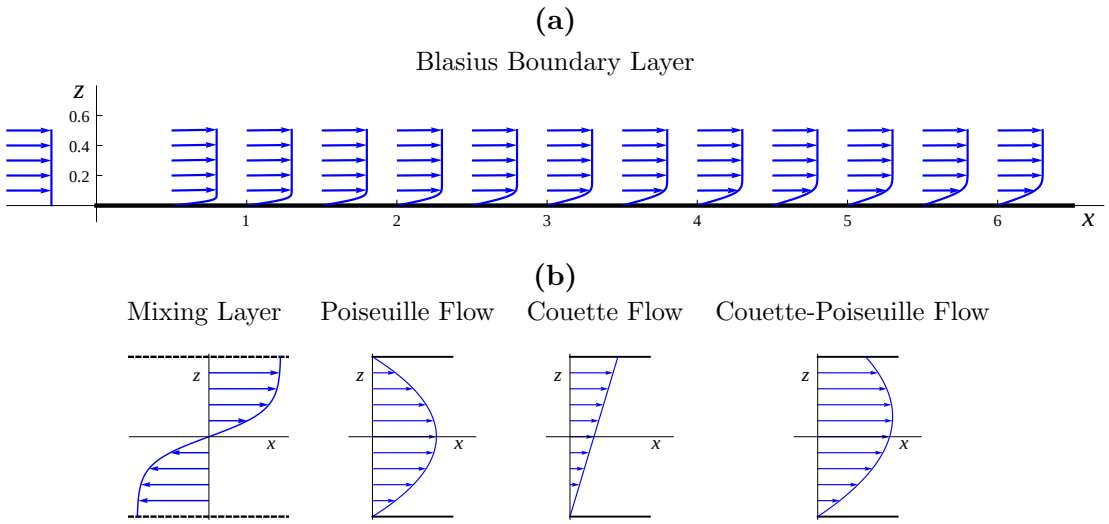

Fig. 2.1 : Examples of 2D ***Open Shear Flows***. **(a)** A slightly non-parallel Flow. **(b)** Parallel Flows.

Finally the unit of time is the advection time, or inertial time, $t_0 = h/U_0$.
The dimensionless form of the Navier-Stokes or Euler equation (2.3) is then

$$\partial_t \overline{\mathbf{u}} + U' u_z \overline{\mathbf{e}}_x + U \partial_x \overline{\mathbf{u}} + (\overline{\mathbf{u}} \cdot \overline{\boldsymbol{\nabla}}) \overline{\mathbf{u}} = -\overline{\boldsymbol{\nabla}} p'' + R^{-1} \overline{\boldsymbol{\Delta}} \overline{\mathbf{u}} \,, \tag{2.6}$$

with[1]

$$\text{the } \textbf{\textit{Reynolds number}} \quad R = U_0 h/\nu \,, \quad R = \infty \text{ in an inviscid fluid.} \tag{2.7}$$

Contrarily to the problem of the Rayleigh-Bénard Thermoconvection which has been studied in the chapter 1, the basic flow creates an anisotropy in the xy plane. Despite this, we assume that it is relevant to focus, firstly, on perturbations that are ***2D xz***. It is convenient then to use a perturbation ***streamfunction*** ψ such that

$$\overline{\mathbf{u}} = \overline{\mathbf{curl}}(\psi \, \overline{\mathbf{e}}_y) = -(\partial_z \psi) \, \overline{\mathbf{e}}_x + (\partial_x \psi) \, \overline{\mathbf{e}}_z \,. \tag{2.8}$$

We also eliminate the pressure by solving, instead of (2.6), the vorticity equation, which reduces to its component in the y direction,

$$\partial_t(-\Delta\psi) + \left[\partial_z\left(\overline{\mathbf{u}} \cdot \overline{\boldsymbol{\nabla}} u_x\right) - \partial_x\left(\overline{\mathbf{u}} \cdot \overline{\boldsymbol{\nabla}} u_z\right)\right] = R^{-1}\Delta(-\Delta\psi) + U\partial_x(\Delta\psi) - U''(\partial_x\psi) \,. \tag{2.9}$$

By introducing the local state vector

$$V = (\psi) \,, \tag{2.10}$$

we obtain that it fulfills

$$\boxed{D \cdot \partial_t V = L_R \cdot V + N_2(V,V)} \tag{2.11}$$

$$\text{with} \quad [D \cdot \partial_t V]_1 = -\Delta \partial_t \psi \,, \quad [L_R \cdot V]_1 = R^{-1}\Delta(-\Delta\psi) + U\partial_x(\Delta\psi) - U''(\partial_x\psi), \tag{2.12a}$$

$$[N_2(V,V)]_1 = \left[\partial_z\left(\overline{\mathbf{u}} \cdot \overline{\boldsymbol{\nabla}} u_x\right) - \partial_x\left(\overline{\mathbf{u}} \cdot \overline{\boldsymbol{\nabla}} u_z\right)\right] \,. \tag{2.12b}$$

The boundary conditions, at the 'plates' located at $z = z_\pm$, are,

$$\text{for a viscous fluid, no-slip,} \quad \overline{\mathbf{u}} = \overline{\mathbf{0}} \iff \partial_x\psi = \partial_z\psi = 0 \,, \tag{2.13}$$

$$\text{for an inviscid fluid, slip,} \quad u_z = 0 \iff \partial_x\psi = 0 \,. \tag{2.14}$$

[1] Do not mingle the main control parameter R of this chapter, the Reynolds number, with the main control parameter R of chapter 1, the Rayleigh number.

2.2 Linear stability analysis of Plane Parallel Flows

This linear analysis relies on the calculation of normal modes of the form

$$V \;=\; (\Psi_n(z))\;\exp(ikx+\sigma t) \;=\; (\Psi_n(z))\;\exp[ik(x-c_r t)]\;\exp(kc_i t) \tag{2.15}$$

with $k \neq 0$ the ***wavenumber***[2], n another label to mark normal modes, σ the temporal eigenvalue. Most often the bulk velocity of the basic flow $\langle U\rangle_z > 0$, hence we expect normal modes that are ***waves*** traveling 'to the right' (in the x direction). For this reason we write

$$\sigma \;=\; -i\omega \;=\; -ikc \tag{2.16}$$

with c the ***complex phase velocity***, $c_r > 0$ (most often) the real phase velocity, $kc_i > 0$ (resp. < 0) the growth rate (resp. damping rate). By inserting the form (2.15) in (2.11) and linearizing, we obtain

$$\boxed{(U-c)\Delta\psi \;-\; U''\psi \;=\; (ikR)^{-1}\Delta\Delta\psi} \tag{2.17}$$

which is the ***Orr - Sommerfeld equation*** in a viscous fluid, ***Rayleigh equation*** in an inviscid fluid ($R=\infty$).
The boundary conditions at $z = z_\pm$, are,

$$\text{for a viscous fluid} \quad , \quad \psi \;=\; \partial_z\psi \;=\; 0\;, \tag{2.18}$$

$$\text{for an inviscid fluid} \quad , \quad \psi \;=\; 0\;. \tag{2.19}$$

2.2.1 Linear stability analysis of Inviscid Plane Parallel Flows

Exercise 2.1 ***Rayleigh's inflection point criterion***

Let us assume that an Inviscid Plane Parallel Flow is unstable. Therefore there exists at least one amplified normal mode (2.15), more simply

$$V \;=\; (\Psi(z))\;\exp[ik(x-c_r t)]\;\exp(kc_i t)\;, \tag{2.20}$$

which corresponds to $c_i > 0$.

1 Express $\Psi''(z)$ as a function of $\Psi(z)$, $U(z)$, $U''(z)$, k and c.

2 By multiplication with a suitable function and integration over $z \in [z_-,z_+]$, show that

$$\int_{z_-}^{z_+} \left(k^2|\Psi(z)|^2 + |\Psi'(z)|^2\right)dz \;+\; \int_{z_-}^{z_+} \frac{U''(z)\;|\Psi(z)|^2}{U(z)-c}dz \;=\; 0$$

and, then,

$$\int_{z_-}^{z_+} \frac{U''(z)\;|\Psi(z)|^2}{|U(z)-c|^2}dz \;=\; 0\;. \tag{2.21}$$

3 Conclude that, if $U'' \neq 0$, U'' must change sign somewhere, i.e. there must exist an ***inflection point*** in the U-profile.

A typical example of an 'inflection-point instability' is the ***Kelvin-Helmholtz instability*** of the ***mixing layer***, which has been already approached in Plaut (2014), see also the animations on http://emmanuelplaut.perso.univ-lorraine.fr/mf/KH.htm.

[2] One can easily show that x-homogeneous modes are all damped.

2.2.2 Linear stability analysis of Viscous Plane Poiseuille Flow

Exercise 2.2 ***Linear stability analysis of Plane Poiseuille Flow with a spectral method***

We analyze the stability of Plane Poiseuille Flow (PPF), $U(z) = 1-z^2$, of a Viscous Fluid. For this purpose we solve the ***Orr - Sommerfeld equation*** (2.17), here rewritten with the temporal eigenvalue σ,

$$\boxed{\sigma D\Psi = -\sigma\Delta\Psi = L_R\Psi = -R^{-1}\Delta\Delta\Psi + ik(U\Delta\Psi - U''\Psi)} \tag{2.22}$$

with

$$\Delta = -k^2 + \frac{d^2}{dz^2} \tag{2.23}$$

and the boundary conditions (2.18),

$$\Psi = \Psi' = 0 \quad \text{if} \quad z = \pm 1\ . \tag{2.24}$$

For this purpose, we use a ***spectral expansion*** of the eigenfunctions $\Psi(z)$, as a sum of simple polynomial functions that fulfill the boundary conditions:

$$\Psi(z) = \sum_{n=1}^{N} \Psi_n F_n(z) \quad \text{with} \quad F_n(z) = (z-1)^2\,(z+1)^2\,T_{2n-2}(z) = (z^2-1)^2\,T_{2n-2}(z)\ , \tag{2.25}$$

T_n the n^{th} Chebyshev polynomial of the first kind, $N = N_z$ the number of z-modes. We retain only the Chebyshev polynomials of even index because we know that the relevant modes correspond to $\Psi(z)$ even under $z \mapsto -z$; we could test a more general expansion...

1 Start a Mathematica code by defining the functions F_n (`F[n,z]` in your code) and the ***Gauss-Lobatto collocation points***

$$z_m = \cos[m\pi/(2N+1)] \quad \text{for} \quad m \in \{1,2,\cdots,N\} \tag{2.26}$$

(`z[m]` in your code). Plot a few functions F_n and the collocation points for various values of N, and comment.

2 By inserting (2.25) in (2.22), we get

$$\sigma \sum_n \Psi_n DF_n(z) = \sum_n \Psi_n LF_n(z)$$

which we want to be fulfilled at the collocation points (2.26):

$$\forall m\ , \quad \sigma \sum_n \Psi_n DF_n(z_m) = \sum_n \Psi_n LF_n(z_m)\ . \tag{2.27}$$

With the vector

$$V = \begin{bmatrix} \Psi_1 \\ . \\ . \\ . \\ \Psi_N \end{bmatrix}\ , \tag{2.28}$$

show that (2.27) can be written under a matrix form

$$\sigma MD \cdot V = ML \cdot V \tag{2.29}$$

$$\text{with } MD_{mn} = \qquad\qquad , \quad ML_{mn} = \qquad\qquad . \tag{2.30}$$

Note that n is a 'column index', m is a 'line index'.

3.a Define in your code the operators D and L acting on a general function Ψ or f,

```
Dop[f_]:= ...
Lop[f_]:= ...
```

Create the matrices MD and ML with the good dimension :

```
MatD = MatL = IdentityMatrix[Nz]
```

then, with a double loop, code the rules (2.30):

```
Do[
   Do[
      MatD[[m,n]] = ... ;
      MatL[[m,n]] = ...
     ,{m,1,Nz}]
  ,{n,1,Nz}]
```

Indication : for the derivatives with respect to z to be correctly computed, do not replace too early z by z_m; do this at the end using the `ReplaceAll` command.

3.b To show clearly the control parameters, define

```
MD[k_] = MatD;  ML[k_,R_] = MatL;
```

4 Define the spectrum of the generalized eigenvalue problem (2.29) as

```
spectrum[k_,R_]:= Eigenvalues[{ML[k,R], MD[k]}]
```

and the eigenvalue of the most relevant mode as

```
sigma1[k_?NumericQ,R_?NumericQ]:= Last[Sort[spectrum[k,R]]]
```

The `?NumericQ` will prevent Mathematica from trying to do formal computations on `sigma1`.
By setting k to a typical value, observe the evolution of the spectrum and of the most relevant eigenvalue as a function of R.
Check that PPF is stable at small R but becomes ***unstable*** at large R.

5 Code with the `FindRoot` command the computation of the neutral Reynolds number $R = R_0(k)$ where

$$\mathrm{Re}[\sigma_1(k,R)] \;=\; 0 \;; \tag{2.31}$$

use

```
R0[k_?NumericQ]:= ...
```

to prevent Mathematica from trying to compute formally $R_0(k)$.
Compute a list of values of $R_0(k)$ and plot the corresponding ***neutral curve***. Comment.

6.a By minimizing $R_0(k)$ with respect to k, compute the ***critical parameters*** k_c, R_c, ω_c and c_c of the bifurcation of PPF to the so-called ***TS waves***:

$$k_c \;=\; \quad , \quad R_c \;=\; \quad , \quad \omega_c \;=\; \quad , \quad c_c \;=\; \quad . \tag{2.32}$$

You will perform ***convergence tests*** by varying the number of modes N_z, for instance, saving your results at given N_z :

```
Put[{Rc,kc,omc},"RckcomcNz"<>ToString[Nz]]
```

then comparing the results obtained with $N_z - 1$ vs N_z modes. For this purpose you will load the previous file with the command

```
{Rcold,kcold,omcold} = Get["RckcomcNz"<>ToString[Nz-1]]
```

A reasonable convergence criterion is that k_c, R_c and ω_c do not change by more than 0.1% with $N_z - 1$ vs N_z modes. Determine the minimum number of modes that satisfies this criterion,

$$N_z \;=\; \quad . \tag{2.33}$$

6.b Explain the physical meaning of the values (2.32) found for k_c and c_c.

7.a With the `Eigenvectors` command, find the vector V (2.28) that represents the ***critical mode*** eigenfunction $\Psi(z)$. By coding the summation (2.25), compute this function $\Psi(z)$.

7.b Compute a streamfunction that represents the PPF with a TS wave

$$\overline{\mathbf{v}} \;=\; \overline{\mathbf{v}}_0 \;+\; \overline{\mathbf{u}} \tag{2.34}$$

with $\overline{\mathbf{u}}$ deriving from

$$\psi \;=\; A\;\Psi(y)\;\exp(ik_c x) \;+\; c.c.\;. \tag{2.35}$$

Here A is a 'small' amplitude that one cannot compute with such a linear theory, and that you will vary.
Use this to plot the streamlines of PPF with a more or less developped TS wave.
Comment these plots, in connection with this citation of Reynolds (1895):

> *'when water is caused by pressure to flow through a uniform smooth pipe,*
> *the motion of the water is* ***direct****, i.e., parallel to the sides of the pipe,*
> *or* ***sinuous****, i.e., crossing and re-crossing the pipe,*
> *according as R is below or above a certain value'.*

Chapter 3

Turbulence modelling - Applications to Wind Energy

This chapter corresponds to the Sessions 3, 4, 5 of 2014-2015.

3.1 Turbulence modelling

For the bibliography, especially concerning the 'old' papers, see Frisch (1995).

3.1.1 General definitions - Experimental results

A basic question is: how to characterize spatial complexity ?

This can be done by studying the ***velocity increments*** and their ***structure functions***, as defined below for a length scale r,

$$\eta \leq r \leq L \ ,$$

with η the Kolmogorov scale[1], L the integral scale[2]. Hereafter u (resp. $\overline{\mathbf{u}}$) denotes one component of (resp. the whole) velocity field. One uses a Reynolds decomposition

$$u \ = \ \langle u \rangle \ + \ u' \tag{3.1}$$

with u' the fluctuating velocity.

Definitions

Velocity increments:

$$u_r(x) := u(x+r) - u(x) \ . \tag{3.2}$$

Structure functions:

$$S^n(r) := \langle (u_r(x))^n \rangle = \langle (u(x+r) - u(x))^n \rangle \ . \tag{3.3}$$

Comments

In principle all can be expressed for vectors: $u \to \overline{\mathbf{u}}$, $x \to \overline{\mathbf{x}}$ and $r \to \overline{\mathbf{r}}$.

[1] Denoted ℓ_K in Plaut (2014).

[2] Denoted ℓ in Plaut (2014).

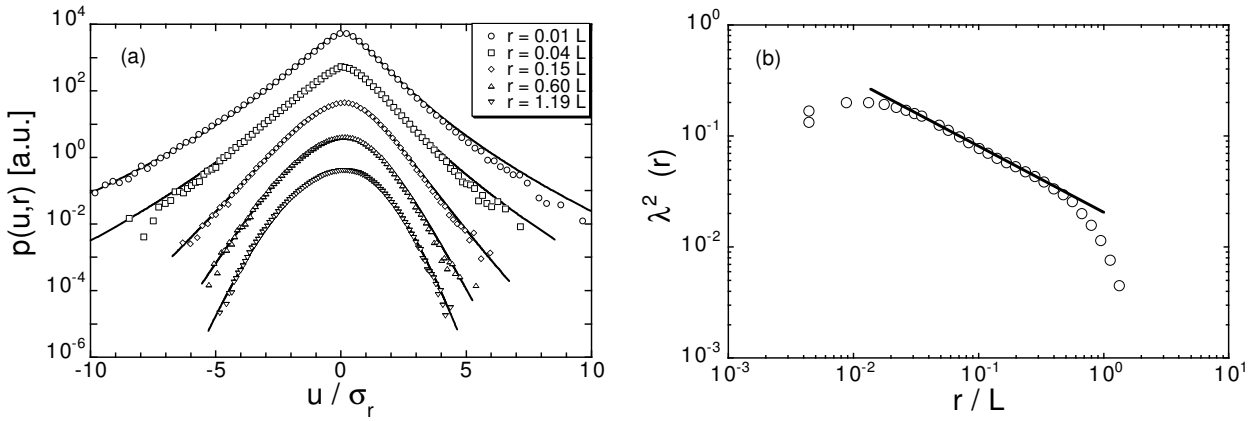

Fig. 3.1 : Statistical analysis of Experimental data acquired with Hot Wire Anemometry on a Laboratory Turbulent Flow, an air into air round free jet (Renner *et al.* 2001; these data are also available on the web page of the module). (a) : PDF $p(u_r)$ of the velocity increments u_r for different values of r; the values of u_r are normalized with the corresponding standard deviation σ_r of u_r. (b) : Corresponding form parameters, see eq. (3.25) below.

Some ***probability density functions*** (PDF) $p(u_r)$ of velocity increments u_r for different values of r are shown in fig. 3.1a. One observes a non-Gaussian character for small values of r, with events corresponding to large increments that are rather 'frequent', at least, with respect to what a Gaussian PDF would give. This is a signature of the ***intermittent character*** of small-scale turbulent flows. Observe that, for larger values of r, the PDF become more and more Gaussian. We will write a model for $p(u_r)$ in section 3.1.4, with the 'multiplicative cascade approach' by Castaing. However, firstly, we present 'older' models that paved the way to arrive to this point of view.

3.1.2 Kolmogorov & Obukov 1941

From the idea of a ***cascade*** Kolmogorov deduced that the structure function should be $S^n(r) = f(\epsilon, r)$ with ϵ the energy (power density) transferred in the cascade. Using dimensional analysis, one gets

$$S^n(r) \;=\; f(\epsilon, r) \;=\; C_n\, \epsilon^{n/3}\, r^{n/3} \tag{3.4}$$

with C_n a universal constant. For $n = 2$ we obtain $S^2(r) \sim r^{2/3}$, and for $n = 3$, $S^3(r) \sim r$, as tested experimentally in fig. 3.2. Note the dimension of the "transferred energy" in the cascade $\epsilon \;\equiv\; E/(t\; m) \;\equiv\; \ell^2/t^3$.

Karmann, Howarth & Kolmogorov derived that form the Navier-Stokes equation and isotropy the so-called $-\frac{4}{5}$***-law***

$$S^3(r) = -\frac{4}{5}\epsilon r + 6\nu \frac{dS^2(r)}{dr}\;. \tag{3.5}$$

According to the eq. (3.4) $6\nu\frac{dS^2(r)}{dr} \propto r^{-1/3}$, thus for large scales ($r \to L$) one has $S^3(L) \propto -\frac{4}{5}\epsilon L$. From this L/η can be estimated. Using

$$\epsilon \;\approx\; \frac{S^3}{L} \;=\; \frac{<(u(x+L)-u(x))^3>}{L} \;\approx\; \frac{<u'^3>}{L}\;, \tag{3.6}$$

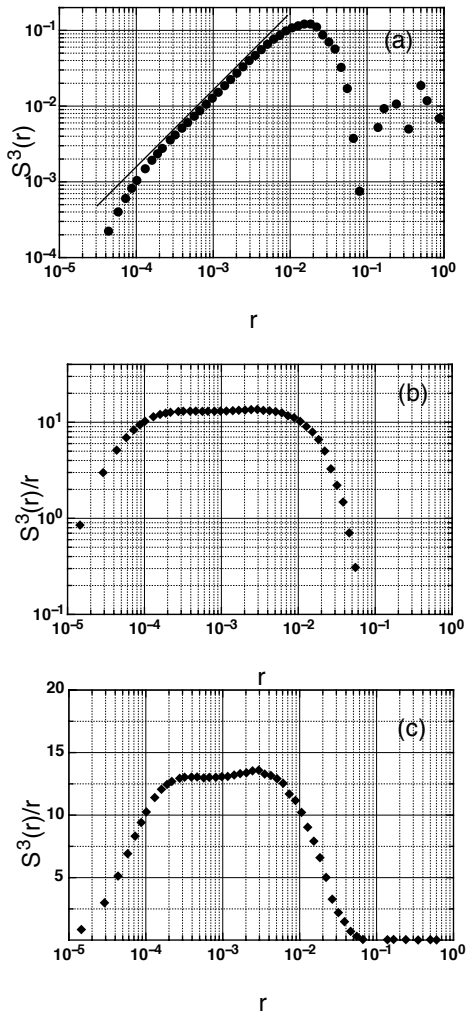

Fig. 3.2 : Experimental test of the law $|S^3| \propto r$, by Chabaud, B. & Chanal, O., CNRS Grenoble, France; reprinted from Friedrich & Peinke (2009). **(a)** Absolute value of the third-order structure function plotted with log-log scales. **(b)** and **(c)** absolute value of the compensated third-order structure function plotted with **(b)** log-log scales **(c)** log-lin scales.

one obtains

$$L/\eta \;=\; \frac{L}{\left(\frac{\nu^3}{\epsilon}\right)^{1/4}} \;=\; \frac{L\epsilon^{1/4}}{\nu^{3/4}} \;\approx\; \frac{L\frac{<u'^3>}{L}^{1/4}}{\nu^{3/4}} \;=\; \left(\frac{u'L}{\nu}\right)^{3/4} \;=\; Re^{3/4}\,. \tag{3.7}$$

3.1.3 Kolmogorov & Obukov 1962

L.D. Landau pointed out that

> *'It is not obvious why ϵ is not a fluctuating quantity'.*

The idea of Kolmogorov 1941 can be taken as $\langle\epsilon_L\rangle = \langle\epsilon_r\rangle = \langle\epsilon_\eta\rangle$ - i.e the mean transfered energy in the cascade is conserved.

After the comment of Landau, Kolmogorov claimed that it is reasonable for $\epsilon(r)$ to assume a ***log-normal distribution***

$$p(\epsilon) \;=\; \frac{1}{\sqrt{2\pi\sigma^2}} \exp\left(-\frac{(\ln x)^2}{2\sigma^2}\right) \;. \tag{3.8}$$

Short argumentation for log-normal distribution

Some notations: The length scales of the turbulent cascade are denoted as $r_n < r_{n-1} < ...r_0 = L$, and $\epsilon_{r_i} := \epsilon_i$ the energy transferred at scale r_i.

The idea of a cascade is that now the sequence of $\epsilon_{r_1} = \epsilon_{r_2} = \ldots = \epsilon_L$ may become random by multipliers such that

$$\epsilon_i \;=\; a_i \; \epsilon_{i-1} \;.$$

The energy conservation is given by the condition $< a_i > \;=\; 1$. Thus one gets for the cascade:

$$\epsilon_{r_n} \;=\; a_n \; \epsilon_{r_{n-1}} \;=\; a_n \; a_{n-1} \epsilon_{r_{n-2}} \;=\; \ldots \;=\; a_n \; a_{n-1} \; \ldots \; a_1 \; \epsilon_L \;. \tag{3.9}$$

Taking the log of this equation:

$$\ln \frac{\epsilon_{r_n}}{\epsilon_L} = \sum_{i=1}^{n} \ln a_i \;. \tag{3.10}$$

This is now taken as a sum over independent random numbers $\ln a_i$. The "central limit theorem" from Kolmogorov says that such a sum of independent random numbers converges towards a Gaussian distribution, hence

$$p(\epsilon_{r_n}) \;=\; p\left(\ln \frac{\epsilon_{r_n}}{\epsilon_L}\right) \;=\; \frac{1}{\sqrt{2\pi\Lambda^2}} \exp\left(-\frac{\left(\ln \frac{\epsilon_{r_n}}{\epsilon_L}\right)^2}{2\Lambda^2}\right) \tag{3.11}$$

where the variance Λ^2 can still be a function of r_n.

Kolmogorov 1962 assumes that

$$\Lambda^2(r) \;=\; \Lambda_0^2 - \mu \ln \frac{r}{L} \;. \tag{3.12}$$

Some argumentation for Kolmogorov 1962 hypothesis

As $\ln a_i$ are assumed to be uncorrelated ($\langle (\ln a_i)(\ln a_j) \rangle = 0$),

$$\Lambda^2(r) \;=\; \left\langle \left(\ln \frac{\epsilon_r}{\epsilon_L}\right)^2 \right\rangle \;=\; \left\langle \left(\sum_{i=1}^{n} \ln a_i\right)^2 \right\rangle \;=\; n \left\langle (\ln a_i)^2 \right\rangle \;\propto\; n \;. \tag{3.13}$$

Thus $\Lambda^2(r) \sim n$ with n the depth of the cascade. Furthermore it is assumed that $r_{n+1} \;=\; k \; r_n$, for example $k \;=\; \frac{1}{2} \quad \rightarrow \quad r_{n+1} \;=\; \frac{1}{2} \; r_n$. Thus

$$\begin{aligned} r_{n+1} \;=\; k \; r_n \quad &\Longleftrightarrow \quad r_n \;=\; k^n \; L \\ &\Longleftrightarrow \quad k^n \;=\; \frac{r_n}{L} \\ &\Longleftrightarrow \quad n \; \ln k \;=\; \ln \frac{r_n}{L} \\ &\Longleftrightarrow \quad n \;=\; \ln \frac{r_n}{L} \; \frac{1}{\ln k} \;. \end{aligned}$$

As $k < 1$, is follows that $\ln k < 0$. Thus we can define $\mu := -\frac{1}{\ln k}$ and one obtains

$$n = -\mu \ln \frac{r}{L} . \tag{3.14}$$

Thus the hypothesis follows

$$\Lambda^2(r) = \Lambda_0^2 - \mu \ln \frac{r}{L} \tag{3.15}$$

with μ an ***intermittency coefficient***.

Knowing $p(\epsilon)$ and $\Lambda^2(r)$ one can calculate

$$\langle \epsilon^{n/3} \rangle \sim r^{-\mu \frac{n(n-3)}{18}} .$$

This is the results of Obukov und Kolmogorov 1962.
One deduces from this that the structure functions

$$S^n(r) = C_n \langle \epsilon^{n/3} \rangle r^{n/3} \sim C_{\epsilon_n} r^{n/3 - \mu \frac{n(n-3)}{18}} \tag{3.16}$$

This equation is known as the intermittency correction to Kolomogov 1941 (3.4). It is easy to see that for $n = 3$ (3.16) the $-\frac{4}{5}$***-law*** is fulfilled, and that

$$S^2(r) = C_{\epsilon_2} r^{2/3 + \mu \frac{1}{9}} , \tag{3.17}$$

$$S^3(r) = C_{\epsilon_3} r , \tag{3.18}$$

$$S^6(r) = C_{\epsilon_6} r^{2-\mu} . \tag{3.19}$$

S^6 is good to estimate the intermittency correction μ.

The structure functions can also be seen as ***spatial 2-point-correlations***,

$$S^n(r) = \langle (u(x+r) - u(x))^n \rangle = \langle u_r^n \rangle = \int_{-\infty}^{\infty} u_r^n p(u_r) du_r . \tag{3.20}$$

Thus the structure functions $S^n(r)$ are the general moments of $p(u_r)$.
If the increments u_r are normalized by $\sqrt{< u_r^2 >}$ to $u_r = \sqrt{< u_r^2 >}\, w_r$ we obtain

$$S^n(r) = \int_{-\infty}^{\infty} u_r^n p(u_r) du_r = < u_r^2 >^{n/2} \int w_r^n P(w_r)\, dw_r . \tag{3.21}$$

If the integral over w_r is independent of r , this is the case if $P(w_r)$ is the same for all r, then Kolmogorv 1941 is obtained again. The other way round, from the intermittency correction, expressed by μ must have the consequence that $P(w_r)$ is changing its from with r.

3.1.4 Multiplicative cascade after Castaing

We follow here Castaing *et al.* (1990). One studies the ***probability density function*** (PDF) $p(u_r)$ of the velocity increments. One can write $p(u_r)$ as function of the conditioned probability $p(u_r|\epsilon_r)$, as

$$p(u_r) = \int_0^{+\infty} p(u,\epsilon_r,r)\, d\epsilon_r = \int_0^{+\infty} p(u_r|\epsilon_r)\, p(\epsilon_r,r)\, d\epsilon_r . \tag{3.22}$$

Castaing assumed (all this is experimentally verified, see e.g. Naert *et al.* 1998) that $p(u_r|\epsilon_r)$ is Gaussian distributed:

$$p(u_r|\epsilon_r,r) \;=\; \frac{1}{\sqrt{2\pi}\,s(\epsilon_r)}\,\exp\left(-\frac{u^2}{2\,s^2(\epsilon_r)}\right)\,. \tag{3.23}$$

Next the standard deviation s depends on ϵ_r as

$$s(\epsilon_r) \;\propto\; \epsilon_r^{\alpha}\,. \tag{3.24}$$

As $\ln(s) \propto \alpha \ln(\epsilon_r)$ also s must be log-normal distributed. Thus

$$p(u_r) \;=\; \frac{1}{2\pi\lambda(r)}\int_{-\infty}^{+\infty}\exp\left(-\frac{\ln^2\left(s/s_0(r)\right)}{2\lambda^2(r)}\right)\exp\left(-\frac{u^2}{2s^2}\right)\frac{d\ln s}{s}\,. \tag{3.25}$$

There are two parameters $s_0(r)$ and $\lambda^2(r)$. The first one $s_0(r)$ is the maximum of the distribution of s and determines the variance of $p(u_r)$. The second one $\lambda^2(r)$ is the variance of the log-normal distribution for s. It determines the form of $p(u_r)$ and is thus called the ***form parameter***. In the limit $\lambda^2(r) \to 0$ a Gaussian distribution is obtained. This is the case for $r > L$, as shows the fig. 3.1a. On the contrary for small scales r the values λ^2 increase thus a departure from Gauss is seen. By fitting the $p(u_r)$, on can estimate the parameter $\lambda^2(r)$ (fig. 3.1b). Thus informations on $\Lambda(r)$ can be obtained, since, as shown in Castaing *et al.* (1990), $\Lambda = 3\lambda$.

3.2 Applications to Wind Energy - Lecture guide

3.2.1 Wind resources (Session 3 of 2014-2015)

One basic aspect of ***wind turbines*** is the knowledge of their energy resource, which is the wind. As turbines are operating in windy places and close to the ground: they take the wind energy in the so called ***'atmospheric boundary layer'*** (ABL). In heights up to a few hundred of meters the atmospheric boundary layer is ***highly turbulent***. It is the structure of the ABL which delivers the wind energy. The next important point will be to understand which conditions this energy resource will deliver to an operating wind turbine. Looking at the response times of the energy conversion process of a wind turbine, it becomes clear that ***turbulent wind fluctuation*** even faster than one second play an important role. Some elements on the modelling of turbulence are given in the previous section 3.1.

The common standard characterization of the wind resource are discussed in a short way in the document **'Characterization of wind turbulence by higher-order statistics'** included hereafter page 27. More details are given in the **Introduction of the PhD Thesis of P. Milan (U. Oldenburg, 2014)** included hereafter page 43. These documents make clear what is taken into account and what is neglected by the standard characterization schemes of turbulent data.

The interested reader will further also read the article by Stresing & Peinke (2010), **Towards a stochastic multi-point description of turbulence**, which is an open-access article. It shows how for idealized laboratory turbulence a general statistical n-point description can be achieved, which also makes clear that there is no simple universal turbulence.

3.2.2 Wind energy basics (Session 4 of 2014-2015)

There we will discuss the ***basic concepts*** of wind energy and the ***working principles*** as well as the ***design*** of a wind turbine. For this refer to the sections 1.3.1 and 1.3.2 of the **Introduction of the PhD Thesis of P. Milan (U. Oldenburg, 2014)** included hereafter page 43.

3.2.3 Conversion dynamics - Power output up to stochastic processes (Session 5 of 2014-2015)

The ***conversion dynamics*** will be explained: the focus will shift to the dynamical aspects. Thus the interaction between the turbulent resource and the turbines will be studied. For an advanced understanding and characterization we need to get into the topic of stochastic processes.
A summary of the mathematics can be found in the **Introduction of the PhD Thesis of P. Milan (U. Oldenburg, 2014)** included hereafter page 43.
Further applications are reported in the article by Wächter *et al.* (2012), **The turbulent nature of the atmospheric boundary layer and its impact on the wind energy conversion process**[3]. The article for further reading by Milan *et al.* (2013), **Turbulent Character of Wind Energy**, discusses the turbulent nature of the wind power in the background of grid integration[4].

[3] Accessible with the information system of University of Lorraine at www.tandfonline.com.bases-doc.univ-lorraine.fr/doi/full/10.1080/14685248.2012.696118 .

[4] Accessible with the information system of University of Lorraine at http://dx.doi.org.bases-doc.univ-lorraine.fr/10.1103/PhysRevLett.110.138701 .

3.3 Applications to Wind Energy - Documents

We include

1. a note **'Characterization of wind turbulence by higher-order statistics'**;
2. hereafter page 43, the **Introduction of the PhD Thesis of P. Milan (U. Oldenburg, 2014)**.

Characterization of wind turbulence by higher-order statistics

Version of January 3, 2015, 10:39

Abstract

We propose a general hierarchical statistical framework for the characterization of wind turbulence to the end that the proper meaning of different statistical approaches and of further developments can be understood. Low order statistical descriptions are extended by higher order statistics with respect to one and two-points. Finally, we give an outlook on how to achieve a general n-point statistical description. In particular we show that proper analysis leads to a super-statistics approach for the probability of velocity fluctuations. To demonstrate the importance of our considerations, we present a synthetic time series using a common software- package (TurbSim). On one side, we show how far this time series is able to reproduce different statistical aspects, on the other side the necessarily of more profound approaches is shown.

based on article: A. Morales, M. W/"achter and J. Peinke : Wind Energy **15**, 391406 (2012)

1 Introduction

Atmospheric wind is not only the source of energy for Wind Energy Converters (WECs), but also the source of mechanical loads which limit the life time of the machines and constrain their operation. In particular wind turbulence leads to power fluctuations, fatigue and extreme loads on WECs. Therefore a thorough description and characterization of wind turbulence is crucial for a reliable design and efficient operation of WECs. On the other hand, due to the presence of many phenomena at many different scales in the atmosphere, a comprehensive and direct analytical description of turbulence remains a challenge.

A way to handle this complexity is to describe the phenomena in terms of statistical quantities. However which statistical information is necessary and sufficient for a certain purpose is not a trivial question. A useful characterization should enable comparison of wind situations between different sites and allow for the adequate selection of a WEC class and layout. The current IEC standard 61400-1:2005 [1] defines a procedure to achieve these requirements based on 10 minute mean values of the wind speed and respective deviations from this mean. Definitions are given for WEC classes, wind situations and probability estimations of certain extreme events. While necessity and usefulness of standards are beyond doubt, in the recent years growing demand for a more comprehensive and more detailed characterization has become evident. This is an active field of research, for example [2] worked on the extreme operative gust and how to incorporate this in the generation of synthetic wind time series. Also recently in [3] calibrations of the extreme cases with return periods of 50 and 1 years in the standard IEC 61400

were presented. Common to the cited works is the explicit role of the particular WEC under consideration. In a more general approach, [4–6] have studied the probability density functions of velocity differences over a range of scales.

This paper tries to review and clarify which kind and which amount of information is grasped by different levels of statistical descriptions of wind turbulence. Our aim is not to give a detailed review of every different statistical approach, but to provide a general and systematic framework which allows to classify and distinguish these approaches and their reach. This is particular important for a systematic review of the statistical methods present in the mentioned IEC norm, while recognizing the value and power of the methods therein but also in the realization of their limitations and where they stand within a systematic and consistent statistical description of wind turbulence.

The structure of the paper is such, that with every section more statistical information for the description of the wind turbulence is taken into account, therefore enhancing the classification of wind turbulence gradually from low order one-point statistics to n^{th}-order two-point statistics. Based on examples we show the suitability and completeness of every step of the statistical description. In section 2 we review the use of one-point statistics. In section 3 two-point statistics of second and higher orders are introduced leading to the necessity of the characterization of intermittency. Finally section 4 adds a note on the generation of intermittency by means of superposition of Gaussian probability density functions (PDFs).

For illustration purposes we use wind data of the research platform FINO I [7]. Trying to avoid wake effects caused by the measurement tower we use data from the top anemometer at 100 m height. The wind speed is recorded with a sampling rate of 1 Hz. For simplicity we work just with the horizontal magnitude $u(t)$ of the wind velocity vector. It is straight forward to extend our scheme to different directional components of the wind vector, as well as to spatial instead of temporal separations.

2 One-Point Statistics

2.1 One-Point Statistics up to Second Order

Given a wind time series, a common approach in the context of wind energy is to define turbulent fluctuations $u'(t)$ superimposed over a mean wind speed [8],

$$u(t) = \langle u \rangle_T + u'(t)_{\langle u \rangle_T}. \tag{1}$$

Here $\langle \cdot \rangle$ denotes time average and T the particular time span taken for calculating the average. In general $\langle x^n \rangle$ is the n^{th} moment of x. These fluctuations around the mean value have themselves a mean value of zero, $\langle u'(t)_{\langle u \rangle_T} \rangle = 0$. Figure 1 (a) shows a typical wind time series and its 10 minute mean values. Figure 1 (b) shows the corresponding fluctuations $u'(t)$. Note that in our notation the index in $u'(t)_{\langle u \rangle_T}$ makes explicit the fact that these fluctuations are always defined through $\langle u \rangle_T$. In our case we take a simple average over the time window T, filtering or more elaborated detrending methods would change the actual value of u' and there statistical properties **??**. Noteworthy is the difference between $u'(t)_{\langle u \rangle_T}$ and $u'(t)_{\langle u \rangle_T} \mid \langle u \rangle_T = \mu$, the latter includes only all those fluctuations that share the same mean value of the wind speed.

One issue with this definition is the need of an averaging period T over which to define the mean wind speed used as reference for the fluctuations. Due to the strong non-stationarity of the wind, this task is not trivial, but 10 minute spans are the usual practice This particular time span is often motivated by the so-called "spectral gap", see [9] for a proper definition. It

is assumed that there is a clear cut between mesoscale variations (large-scale meteorological patterns) and high frequency fluctuations. However, the existence of this gap is arguable [10], and it might not exist clearly for many sites. It could also be argued that WECs can follow adiabatically changes in the wind acting in these or larger time scales. In this way one might propose a WEC based time span T. For simplicity, from now on we will just write $u'(t)$ for $u'(t)_{\langle u\rangle_T}$, and we will also adopt the usual $T = 10\,min$. Our following arguments could be applied to any other characteristic or desired value of T.

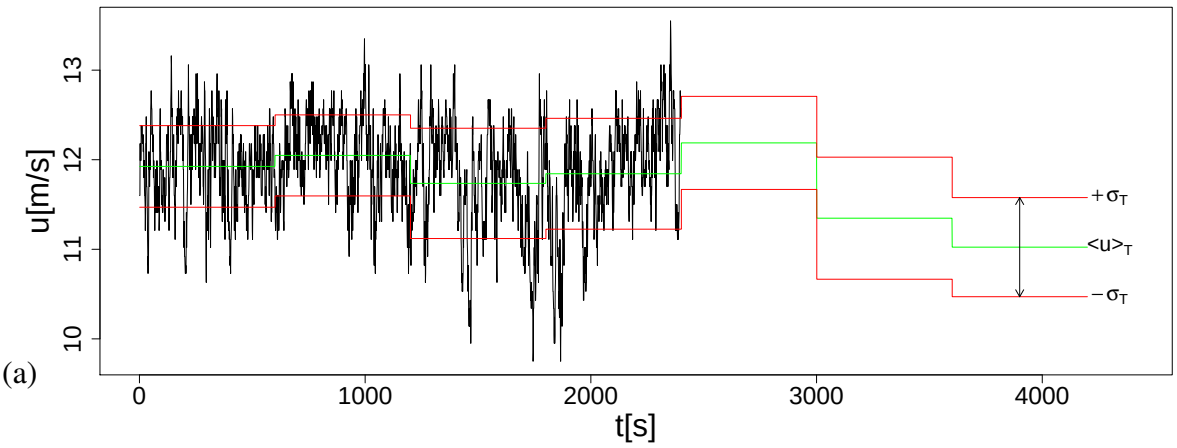

(a)

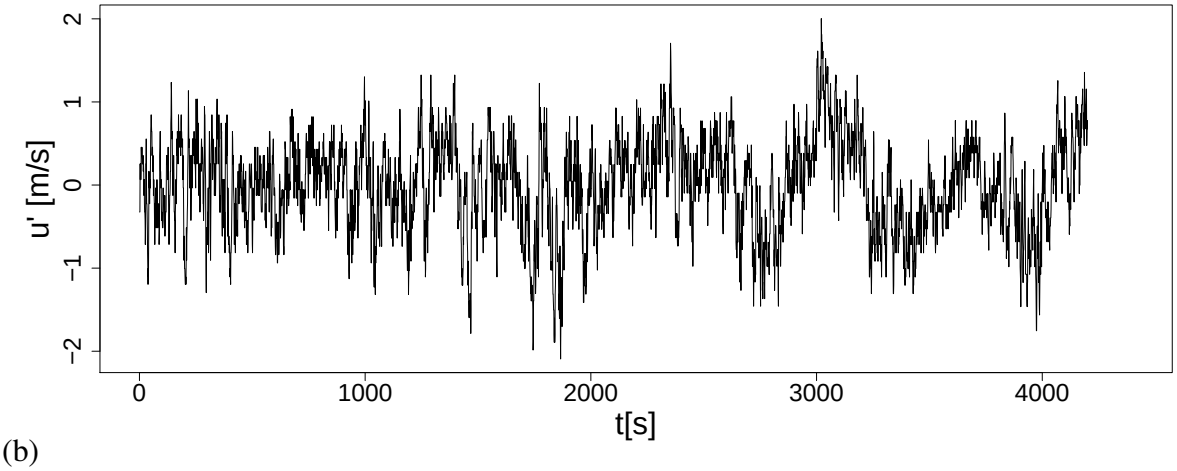

(b)

Figure 1: (a) Time series of the horizontal wind speed $u(t)$ measured on the research platform FINO I at $100\,m$ height, with 10-minute mean values and standard deviations. (b) Fluctuations $u'(t)$ defined over 10-minute mean values.

In this context, an estimation of turbulence strength in the wind during the time span T is the turbulence intensity

$$I = \frac{\sqrt{\langle u'^2\rangle_T}}{\langle u\rangle_T} = \frac{\sigma_T}{\langle u\rangle_{10min}}\,. \tag{2}$$

Here σ_T is the standard deviation of the fluctuations departing from the mean wind speed in the considered period of time. The turbulence intensity is a crucial parameter by which, e.g., certification and site assessment procedures are defined, and it is indeed a design constraint [1]. Details on how this parameter changes with height, mean wind speed or surface roughness can

be found for example in [1, 11] and for offshore data in [12]. As important as it is, the statistical information in this parameter is restricted to the standard deviation or the second moment of the fluctuations. Formally the statistics contained in the turbulence intensity are one-point statistics of second order. As we will introduce in the next section, higher order moments of the fluctuations, $\langle u'^n \rangle$ with $n > 2$, are necessary for the description of extreme values of u'.

2.2 Higher Order One-Point Statistics

In the previous subsection we discussed first-order ($\langle u \rangle_{10min}$) and second-order ($\sigma_T$) one point statistics, which are summarized in the turbulence Intensity I. In General higher order moments are also significant, and this information is contained in the form of the probability density function (PDF) of fluctuations. As $\langle x^n \rangle = \int x^n p(x) dx$, the complete set of moments is contained in the knowledge of the PDF of a statistical quantity. The only case where the first two moments will give a complete description of one-point statistics, is the case where the PDF of the fluctuations follows a Gaussian distribution, since only this distribution is completely defined by its first two moments.

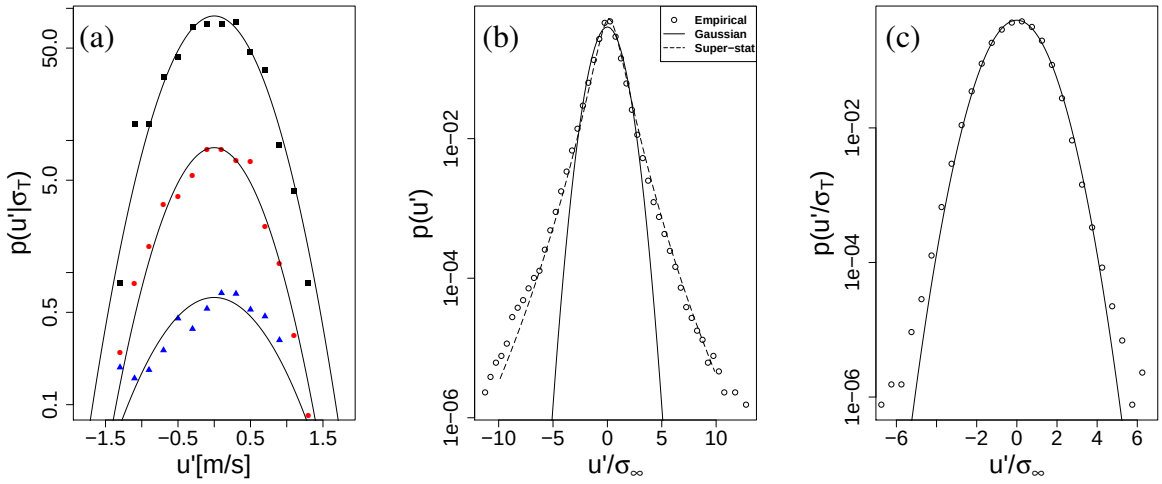

Figure 2: (a) $p(u'(t)|\sigma_T)$ for three arbitrary ten-minute intervals. From top to bottom the values of the respective σ_T are 0.456, 0.452 and 0.616 m/s, the flatness $\langle u'^4 \rangle / \sigma_T^4$ are 2.82, 2.82, and 2.89 ± 0.79. (b) PDF of $u'(t)$ considering all the data set. The flatness is 6.30 ± 0.11, and $\langle (ln\sigma'_T - \overline{ln\sigma'_T})^2 \rangle = 0.2037$. (c) PDF of $u'(t)/\sigma_T$ where σ_T is the standard deviation in each interval of length T. Flatness is 2.98 ± 0.01. Symbols represent wind data and solid lines Gaussian distributions in all figures.

Thus the question whether wind fluctuations follow a Gaussian distribution or not becomes relevant in order to understand how much a parameter like the turbulence intensity I characterizes such fluctuations. To consider the Gaussianity of the fluctuations, figure 2 presents the PDFs for different sets of $u'(t)$. Figure 2 (a) shows the PDFs for some arbitrary single 10-minute intervals. Which can be understood as $p(u'(t)|\sigma_T^i)$, where σ_T^i denotes the standard deviation of the i^{th} 10-minute interval. Within such intervals fluctuations seem to follow the Gaussian distribution, and the pdfs can be characterized by the corresponding σ_T^i. In contrast to this in figure 2 (b) the complete set (20 days) of $u'(t)$ is shown. We see that in this case the probabilities of large values of fluctuations are clearly underestimated by a Gaussian dis-

tribution. Note the logarithmic y-axis, for example a 10σ event would be underestimated by a Gaussian distribution by a factor of 10^8.

Finally figure 2 (c) shows again the PDF of the total data set, but here in each i^{th} ten minute interval the fluctuations $u'(t)$ were normalized by the corresponding σ_T^i standard deviation of the respective i^{th} 10-min interval. The resulting PDF $p(u'(t)/\sigma_T^i)$ is well described by a Gaussian distribution within $\pm 5\sigma$. Small deviations may be seen for the largest values, but the significance here is rather questionable. Nevertheless comparing figure 2 (b) and (c) we clearly see that for $p(u'(t)/\sigma_T^i)$ a Gaussian distribution is a very good approximation.

These findings support the hypothesis that $u'(t)$ is Gaussian distributed within ten minute intervals, but with different standard deviations σ_T for each interval. It is known that the standard deviations σ_T of $u'(t)$ for single ten-minute intervals are closely log-normal distributed and the parameters of the log-normal distributions depend on the mean wind speed [11]. Thus if fluctuations $u'(t)$ are considered without normalization , the superposition of the different Gaussians distributions with different σ_T leads to the intermittent distribution in figure 2 (b).

For a more quantitative evaluation of deviations from Gaussianity, it is common to calculate the third and fourth moments of the fluctuations normalized by the standard deviation, which are called skewness *Skew* and flatness F, respectively. For a general signal $x(t)$ the definitions are

$$Skew(x) = \frac{\langle (x-\bar{x})^3 \rangle}{\sigma_x^3} \tag{3}$$

$$F(x) = \frac{\langle (x-\bar{x})^4 \rangle}{\sigma_x^4}\,. \tag{4}$$

A Gaussian distribution has a skewness value of zero and a flatness of three. For all the cases in figure 2, the values of the skewness do not differ significantly from zero, confirming the symmetry of the distributions. The values of the flatness are 2.82, 2.82, and 2.89 ± 0.79 from top to bottom in figure 2 (a) and thus do not contradict the Gaussian distribution for arbitrary single ten-minute intervals, while the large deviations from Gaussianity in figure 2 (b) result in a flatness of 6.30 ± 0.11. For the PDF of all the normalized ten-minute intervals in figure 2 (c) the flatness of 2.98 ± 0.01 is again close to the Gaussian value.

From the discussion above it follows that an assumption of Gaussianity for $u'(t)$ holds only for single ten-minute intervals, and caution should be taken when estimating the probability of extreme values of u'. And in general higher moments than $\langle u'^2 \rangle$, or related quantities like the flatness (see eq. (4)), will be needed for a correct description of $p(u')$. This non-Gaussianity of the extreme excursions from the mean wind speed has been already noted in, e.g., [13]. More recently in [14] an asymptotic expression for describing the distribution of such extreme events was presented.

Based on our above findings that $p(u'(t)|\sigma_T)$ is Gaussian we can apply a superposition approach similar to [15] like,

$$p(u') = \int p(u'|\sigma_T') \cdot p(\sigma_T') d\sigma_T'. \tag{5}$$

Here $p(u'|\sigma_T')$ represents a Gaussian distribution and $p(\sigma_T')$ a log-normal distribution. The key parameter is $\langle (ln\sigma_T' - \overline{ln\sigma_T'})^2 \rangle$ which gives directly a measurement of the intermittency of $p(u')$ and is therefore actually related to the flatness of the distribution. Figure 2(b) shows that our model based on equation 5 is able to describe the PDF $p(u')$ properly in all the range of fluctuations. Further details on this approach can be found in [16], but we want to note that in

principle additional dependencies of $p(u')$ on mean wind speed, height, and site can be easily grasped by the respective value of $\langle(ln\sigma'_T - \overline{ln\sigma'_T})^2\rangle$.

Up to this point we have been discussing stepwise one-point statistics of first order $\langle u\rangle$, of second order in σ_T, and of higher orders summarized in the PDF of u'. However even a complete knowledge of $p(u')$, or respectively of all the moments $\langle u'^n\rangle$, is not unique in the sense that many different time series can share these statistics. To make this point more clear we refer to figure 3, which shows three time series which have Gaussian distributions $p(u')$. Those time series share the same one-point statistics, thus the same value of standard deviation and will give the same value of turbulence intensity once added to the same mean wind speed. And clearly the nature of these time series is different.

This is not surprising since the PDF of $u'(t)$ gives no information regarding which path the process follows in order to achieve the observed distribution. In order to distinguish more features of the time series a proper correlation analysis is necessary. The next section will therefore deal with the characterization of correlations by two-point statistics.

3 Two-point statistics

3.1 Two-point statistics up to second order

As seen in the previous section and in figure 3 it is in general neccesary to obtain knowledge on the correlations between two points in the time series of wind fluctuations. The basic statistical tool for this purpose is the autocorrelation function

$$R_{u'u'}(\tau) = \frac{1}{\sigma^2_{u'}} \left\langle u'(t+\tau)\, u'(t) \right\rangle \tag{6}$$

which quantifies the correlation of two data points separated by the time lag τ. The Wiener-Khintchine theorem [17] relates it to the power spectral density $S(f)$ via a Fourier Transformation $\mathcal{F}$, thus both functions contain the same information:

$$S(f) \overset{\mathcal{F}}{\Longleftrightarrow} R_{u'u'}(\tau) \quad \text{with} \quad \sigma^2_{u'} = \int S(f)\mathrm{d}f\,. \tag{7}$$

These are second order two-point statistics and give information on the intensity or amplitude with which different frequencies contribute to the fluctuations. This statistical tool already enables us to distinguish between the signals shown in figure 3 despite that they share the same one-point statistics. As we can see in figure 3 in the case of the random signal our description would be complete with the turbulence intensity because the PDFs of the fluctuations are Gaussian and the fluctuations are completely uncorrelated, i.e.,

$$R_{u'u'}(\tau) = \delta(\tau). \tag{8}$$

However as we know this special case would be very difficult to find in the atmosphere where many different interactions occur over many scales [9]. Instead as can be seen again in figure 3 the atmospheric turbulence exhibits a lot of structure regarding the power spectrum. In the so-called inertial range usually a Kolmogorov similarity theory is adopted in order to explain the spectrum over a range of frequencies ($S(f) \propto f^{-5/3}$). In practice either the Kaimal or the von Karman spectra are used not only for the description of atmospheric turbulence but also in the generation of synthetic wind fields [18].

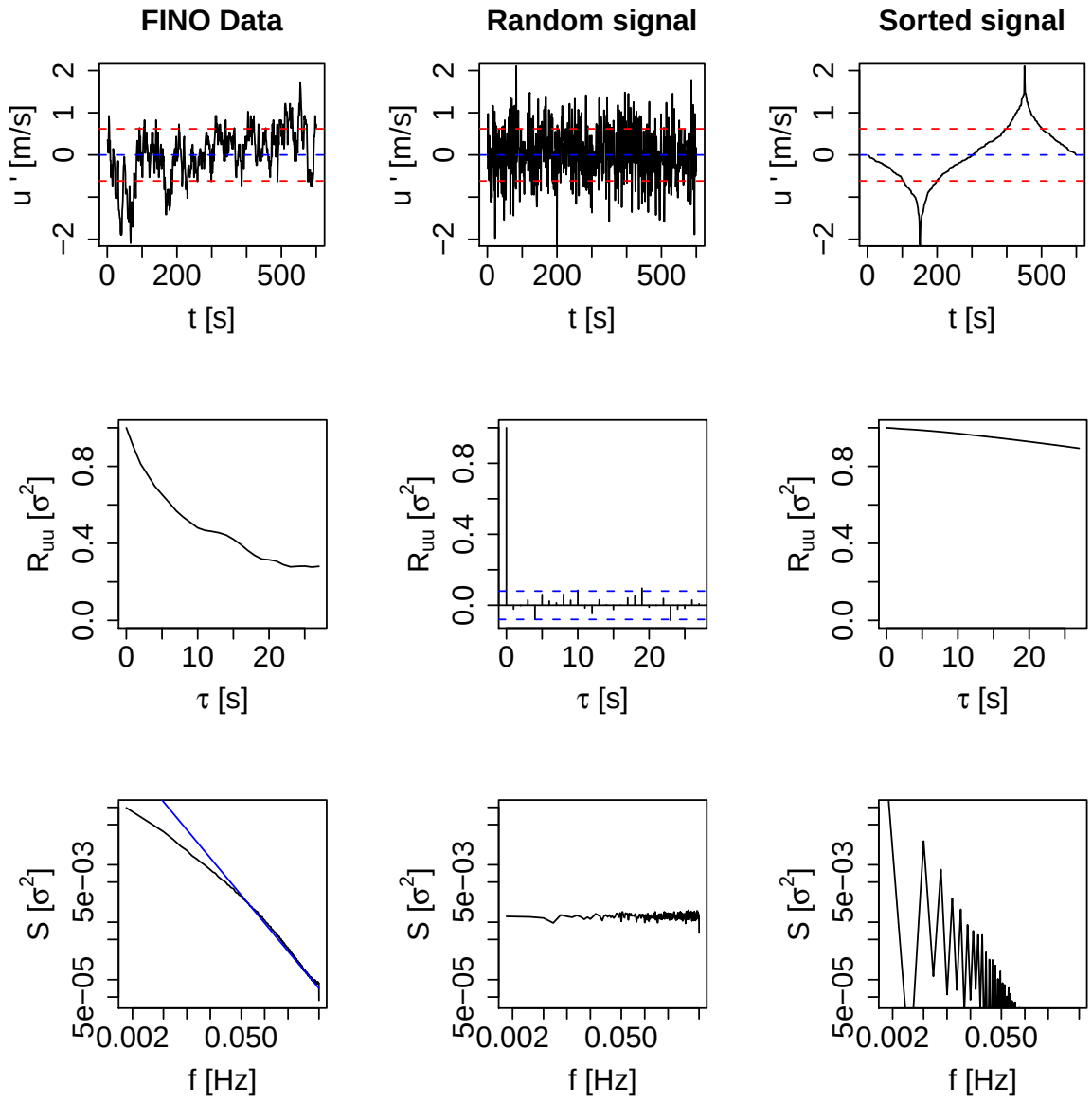

Figure 3: Three different time series, their autocorrelation functions $R_{u'u'}(\tau) = \langle u'(t+\tau)u'(t)\rangle$, and power spectral densities $S(f)$. From left to right, atmospheric fluctuations u' (measured at FINO I), a random Gaussian distributed time series, and an ordered time series constructed from the random series. All three share the same standard deviation σ_T, and closely the same $p(u')$. In the top column the dashed lines correspond to one standard deviation. The straight line shown with the FINO 1 power spectral density corresponds to $S(f) \propto f^{-5/3}$. From the figure it is clear how even a complete knowledge of one-point statistics is not sufficient in order to characterize wind turbulence.

Similar to the one-point statistics up to second-order summarized in the turbulence intensity I, the autocorrelation function and the power spectral density are important and widely used statistical quantities. Nevertheless, in the general case higher order two-point statistics are indispensable. In principle we should ask ourselves for higher correlations of the form,

$$R_{u'^n u'^m}(\tau) = \frac{1}{\sigma_{u'}^{n+m}} \left\langle u'(t+\tau)^n \, u'(t)^m \right\rangle . \tag{9}$$

However, it is more general and even practical to work with the statistics of wind speed differences. As we will see in the next subsection these are also two-point statistics and their moments contain the arbitrary order two-point correlations defined in Eq. (9). These will be discussed in the next subsection in terms of wind speed differences.

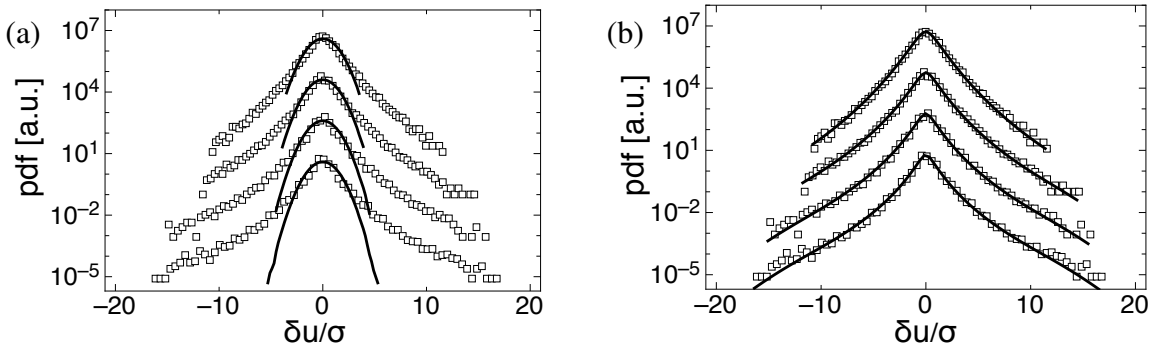

Figure 4: PDFs of wind speed increments, $\delta u(t,\tau)$, displayed by symbols and shifted vertically. Scales from bottom to top are $\tau = 2$, 4, 10, and 60 s. Additionally, the PDFs are modeled by (a) Gaussian distributions with identical standard deviations, and (b) Castaing's formula (12) with (13) and (14).

3.2 Higher-order two-point statistics

To investigate more generally two-point statistics and higher order correlations in wind turbulence, let us now consider wind speed differences over a specific time lag τ,

$$\delta u(t,\tau) = u(t+\tau) - u(t) = u'(t+\tau) - u'(t) , \tag{10}$$

which we will refer to as *wind speed increments* in the following. Wind speed increments statistics are clearly by definition two-point statistics, and the necessity of selecting a time span for calculating the mean wind speed is avoided. Instead the increments are defined over a scale τ, and the nature of wind speed variations can be studied against the evolution of this scale. The increment's second moment is directly connected to $R_{uu}(\tau)$ by the simple calculation

$$\langle \delta u(t,\tau)^2 \rangle = 2\langle u(t)^2 \rangle - 2\langle u(t)\, u(t+\tau) \rangle = 2\langle u(t)^2 \rangle \, (1 - R_{uu}(\tau)) , \tag{11}$$

assumed that the time series is long enough to ensure $\langle u(t)^2 \rangle = \langle u(t+\tau)^2 \rangle$ within the desired precision. Note that these considerations apply for the wind speeds $u(t)$ as well as for their fluctuations $u'(t)$, at least inside a ten minute interval, see Eq. (10). Thus, from the power spectral density and autocorrelation function we obtain the variances or the second moment of the wind speed increments as a function of τ. It is straight forward to see that higher moments of

wind speed increments, $\langle \delta u(t,\tau)^n \rangle$ with $n > 2$, are related to higher order correlations, compare with Eq. (9).

In figure 4 (a) we show PDFs of wind speed increments for different time scales τ, together with Gaussian PDFs which share the same standard deviation. Typically PDFs of atmospheric wind speed increments are non-Gaussian for a wide range of scales and have a special "heavy-tailed" shape [4] (e.g., figure 4). As already noted in section 2, the Gaussian distribution is the only one completely determined by the first two moments. Therefore it becomes clear that for wind speed increments the knowledge of higher-order moments than the second is necessary for a proper characterization of their PDFs. This is a well known and heavily discussed phenomena for turbulence [19] and this is analogous to the case presented in subsection 2.2, where we found that higher moments of one-point statistics $\langle u'^n \rangle$ were needed in order to describe the corresponding u' PDFs. AgaThe observed tails in the PDFs imply an increased probability of extreme events, as much as several orders of magnitudes, compared to a Gaussian distribution. Therefore these tails have to be properly reflected in the statistical description.

To this end we follow [4] and parameterize the PDFs using Castaing's model [15], which with some minor modifications is also an explicit formula for Eq. (5)

$$p(\delta u(\tau)) = \frac{1}{2\pi\lambda(\tau)} \int_0^\infty \frac{\mathrm{d}\sigma}{\sigma^2} \exp\left[-\frac{\delta u(\tau)^2}{2\sigma^2}\right] \exp\left[-\frac{ln^2(\sigma/\sigma_0)}{2\lambda^2(\tau)}\right]. \tag{12}$$

In this equation the PDF is considered as a continuous superposition of Gaussian distributions with different standard deviations, which are weighted by a log-normal distribution function. The shape of the resulting PDF is determined by the two parameters $\lambda^2(\tau)$ and σ_0. Here, σ_0 fixes the median of the lognormal function, while $\lambda^2(\tau)$ mainly dictates the shape of the distribution and is accordingly called the shape parameter. $\lambda^2(\tau)$ is zero for Gaussian distributions and for positive values intermittent distributions are achieved. In general for an emprically given PDF, both parameters can be estimated straightforwardly by an optimization procedure based on equation (12). Beck [20] showed that for the case when log-normal superstatistics is the right model, then $\lambda^2(\tau)$ can be directly estimated from the flatness. Following such procedure for Eq. (12) we obtain

$$\lambda^2(\tau) = \frac{ln\left(F_{\delta u}(\tau)/3\right)}{4} \tag{13}$$

where $F_{\delta u}(\tau)$ is the flatness of the increment PDF at a given scale τ, cf. equation (4). Considering the moments of Gaussian and log-normal distributions we obtain for σ_0, also from [20],

$$\sigma_0^2 = \langle \delta u(\tau)^2 \rangle \exp\left[-2\lambda^2(\tau)\right]. \tag{14}$$

In figure 4 (b) we model the PDFs by Castaing's formula (12), using (13) and (14) for a simplified estimation of $\lambda^2(\tau)$ and σ_0. It can be seen that the measured increment PDFs are well reproduced for all scales τ.

Now, in figure 6 we show how the shape parameter behaves against the scale τ for our offshore data. It is important to note the difference between unconditioned and conditioned (by a mean wind speed bin) values of atmospheric data. The behavior of the PDFs or respectively of $\lambda^2(\tau)$ against scale is similar, but the conditioned PDFs show a reduced overall intermittency. The reduction of intermittency for conditioned data sets is due to the fact that part of this intermittency stems from the non-stationarity of the wind. Indeed [5] has already noted the importance of the non-stationarity of the mean wind speed in the increments' PDFs and developed an elaborated model. This model takes into account the variation of the 10 mins. mean wind speeds by considering their Weibull distribution. Also in the cited work [5], a more

comprehensive and elaborated analysis was already given for $\lambda^2(\tau)$. Studies for different types of terrain (and also laboratory data) were carried out, and in general for atmospheric data the same strong and robust intermittency over a large range of scales was found.

Regardless of the absolute value of $\lambda(\tau)$ it is important to note that, for both the conditioned and unconditioned sets, there is a clear range of scales τ where $\lambda^2(\tau) \sim \ln\tau$. This logarithmic dependency has a deep meaning in turbulence and is directly related to the intermittency correction of turbulence in the Kolmogorov 62 theory [19]. In particular with

$$\lambda^2(\tau) \approx \lambda_0^2 - \mu \cdot \ln\tau, \tag{15}$$

and using Eq. (12) one gets

$$\langle \delta u(\tau)^n \rangle \propto \tau^{\frac{n}{3} - \mu\frac{n(n-3)}{18}}, \tag{16}$$

which is the well known multifractal behaviour of turbulence [19].

In summary we have found that higher moments of the increments are neccessary for the proper estimation of the wind speed increments $\delta u(\tau)$ PDFs, in particular for the correct estimation of extreme events. Fortunately in many cases with $\sigma_{\delta u}(\tau)$ and $F_{\delta u}(\tau)$, we achieve a precise estimation of arbitrary-order two-point statistics of the wind speed. The according wind speed increment PDFs can be modeled following equations (12) to (14).

4 Synthetic time series vs Atmospheric Turbulence

In the previous sections we have hierarchically presented a statistical description of atmospheric turbulence. We have seen that in general atmospheric turbulence contains relevant information in higher-order moments of both one- and two-point statistics. A nice way to summarize and contrast this with what is usually standard and used in the wind energy industry, is by the use of a standard software used for the synthetic generation of turbulent wind fields. In particular we use the TurbSim [21] package. With this package it is possible to generate a synthetic time series wich contains one-point statistics (at all orders) and two-point statistics up to second order in a very similar way to the statistics of a conditioned FINO data set (we use 10-minute time intervals which fullfill $\langle u \rangle_T = 10 \pm 1\, m/s$). In particular we generate a synthetic wind time series, in such a way that $p(u')$ reproduces the behavior of the conditioned FINO data set. We achieve this by generating with TurbSim Gaussian 10-mins. intervals $p(u'|\sigma'_T)$, with the constraint that the different σ'_T of each 10-mins. interval follows the distribution $p(\sigma'_T)$ of the conditioned FINO data set (compare with subsection 2.2). Note that the TurbSim method allows to follow a Kaimal power spectral density, thus the spectrum of the synthetic time series follows a law $S(f) \propto f^{-5/3}$ for high frequencies by default. Thus the synthetic time series reproduce $p(u')$ (complete one-point statistics) and $S(f)$ (two-point statistics up to second order) of the atmospheric data set closely as seen in figure 5. On the other hand, when we analyse higher-order two-point statistics, summarized in the behavior of λ^2 against scale τ, we find that the synthetic time series do not reproduce properly the wind PDFs (see figure 6). The synthetic time series understimate consistently the probability of extreme events, and in contrast to the atmospheric behavior there is no real evolution of λ^2 against the time step τ.

As discussed in the previous section, the exact dependency of λ^2 against τ, expressed in Eq. (15), has an important physical meaning. The failure in reproducing such behaviour by the synthetic time series can not be ignored and represents and important weakness of the models. To summarize this example, we showed that the higher-order two-points statistical information, which is characterized by $\lambda^2(\tau)$, can not be obtained by means of even a complete knowledge of one-point statistics and the spectral density.

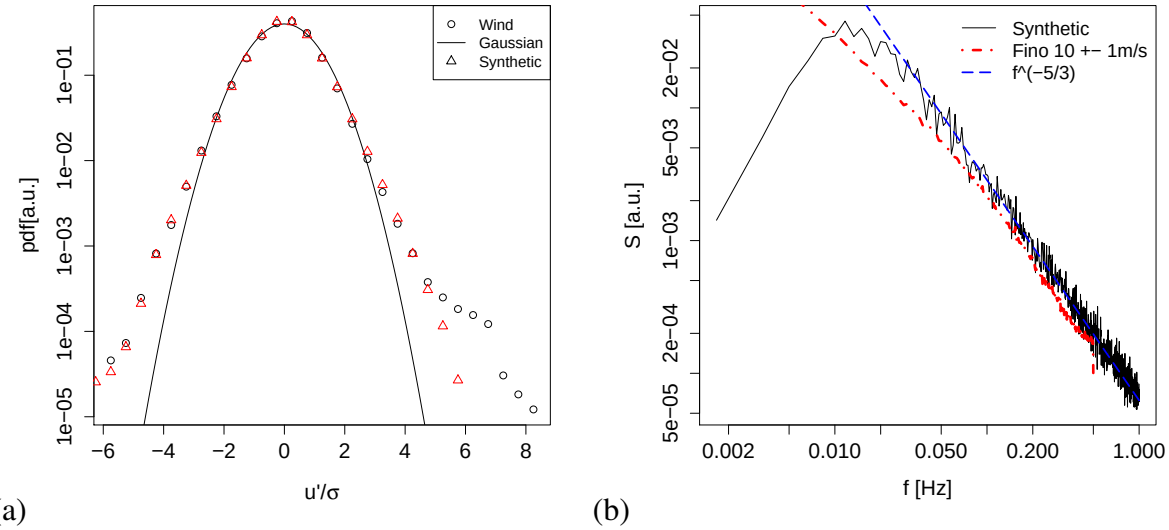

(a) (b)

Figure 5: Basic (a) PDF of $u'(t)$. (b) Normalized FINO and Synthetic spectral densities. A curve following $S \propto f^{-5/3}$ has been added for comparison.

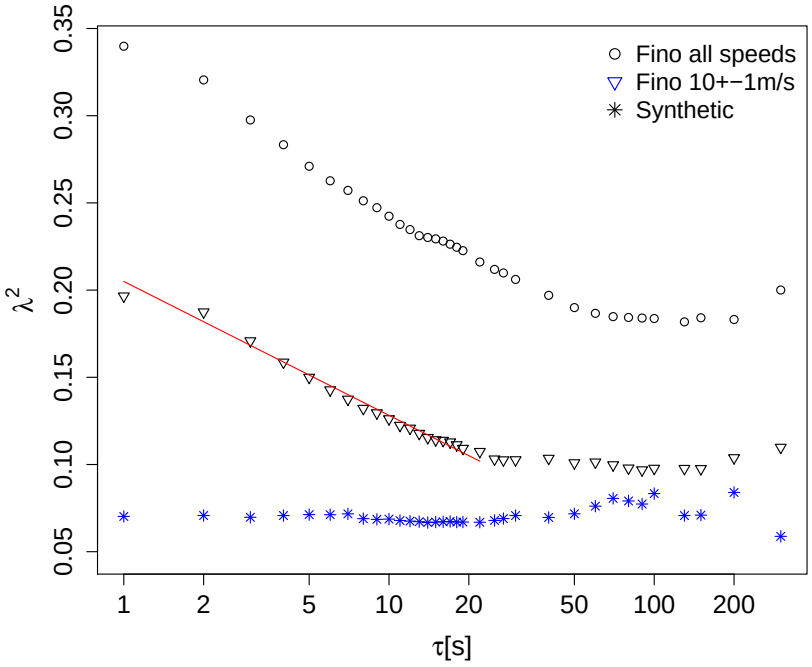

Figure 6: $\lambda^2(\tau)$ against τ for all wind speeds of the data set ($\triangle$), for wind speeds of $(10 \pm 1)\, m/s$ ($\bullet$), and for a synthetic time series ($*$, see text).

5 Outlook: n-point statistics

In the previous section we proposed a comprehensive characterization of increments PDFs by the shape parameter $\lambda(\tau)$. These increment PDFs provide information on arbitrary-order two-point correlations. However, to give one example gust clustering and its prediction can not be achieved with the mentioned statistical information. The natural next step in our hierarchical description would be the study of n-point statistics. The complete stochastic information is contained in the general n-point joint PDF,

$$p(u_{\tau_1}, u_{\tau_2}, ..., u_{\tau_n}). \tag{17}$$

Those PDFs quantify the probability that at the same time the wind speed differences $u_{\tau_1}, u_{\tau_2}, ..., u_{\tau_n}$ are observed on the scales $\tau_1, ..., \tau_n$. While the increment PDFs presented in the previous section characterize arbitrary-order two-point correlations, these n-point joint PDFs defined in eq. (17) would capture the arbitrary-order n-point correlations [22]. Specific wind gust shapes should be, in principle, characterized by these type of statistics. Up to now, the characteristic wind gust shapes mentioned in the IEC standard 61400-1:2005 [1] are treated in a rather deterministic way. Capturing a more stochastic, realistic, n-point information would imply a further step in our proposed characterization scheme. Up to our knowledge not many works have been carried out in this direction and more work has to be carried out.

6 Conclusions

A statistical characterization of wind turbulence has been presented in a hierarchical and mathematical consistent way. In doing so, we have reviewed the well known one-point statistics up to second order summarized in the so called turbulence intensity as well as the two-point statistics up to second order reflected in the spectral density. We have shown that in general, in the case of wind speed time series, higher order moments contain relevant statistical information in both one and two-point statistics and can not be ignored. Therefore we propose to use the probability density functions of wind speed fluctuations u' and wind speed increments $\delta u(t, \tau)$ in order to grasp the statistical information of higher-moments. In the case of the fluctuations u' we have presented a superposition model which manages to describe the measured PDFs rather well. A similar approach is used for the increments statistics, historically this approach has been already applied in laboratory turbulence by [15] and for atmospheric turbulence by [5]. Here the method has been applied to wind speed fluctuations (u') leading to a new superposition approach of $p(u')$. For the characterization of wind speed increments $\delta u(t, \tau)$ it is in many cases possible to characterize these increment PDFs just by the second and fourth moment (this has to be done in a careful way by checking the quality of this approach like in Fig. 4.). From these the so-called shape parameter $\lambda(\tau)$ is crucial in the characterization. We would like to note that the current practice in wind energy assessment and according regulations [23] do not include the characterization of higher-order two point statistics. An easy improvement in the assessment of turbulent conditions would be the systematic estimation of the shape parameter as a function of τ. Of course a question of special practical importance is which scales τ are relevant for WECs. It seems reasonable to expect that these critical scales will depend on every type of machine. However, as shown here (even with a superposition approach for the fluctuations u') and in [24] common models and simulation packages for generating synthetic wind fields do not reproduce these two-point statistics. As a consequence, quantitative evaluations of possible effects on WECs due to the non-Gaussian behavior of wind speed increments have not

been carried out until very recently [24]. Finally, future investigatons should focus on n-point statistics for the characterization of, e.g., gust clustering and the identification of critical wind gusts shapes. This will imply further investigations in our proposed characterization scheme.

Table 1 presents a summary of the observed statistical features of the wind, as well as the statistical quantities to characterize them. Additionally columns for time series generated by spectral models and a random time series (compare figure 3) are presented, showing how much of the statistical information they contain.

Table 1: Turbulence Characterization Scheme

Type of Statistics	Order	Feature	Random Data	Spectral Models	Wind Turbulence	Characterization
1-point	1	Mean speed	•	•	•	$\bar{u} = \langle u(t) \rangle_T$
	2	Turbulence Intensity	•	•	•	$I = \sigma_{u'}/\bar{u}$
	n	Extreme Fluctuations	-	$*^a$	•	$p(u')$
2-point	2	Distribution of σ_u over f	-	•	•	$S(f) = \mathcal{F}\{R_{uu}(\tau)\}$
	n	Intermittency of $p(\delta u(\tau))$	-	-	•	$\lambda(\tau)$
n-point	n	Arbitrary-order n-point correlations	-	-	•	To be investigated

[a] Achievable via a superposition approach. See section 4

References

[1] IEC: Wind Turbines Part 1: Design requirements. International Standard 61400-1:2005, International Electrotechnical Commission, 2005.

[2] Bierbooms W: *Constrained Stochastic Simulation of Wind Gusts for Wind Turbine Design*. Ph.D. thesis, Delft University Wind Energy Research Institute, 2009.

[3] Larsen GC, Hansen KS: Rational calibration of four iec research 61400-1 extreme external conditions. *Wind Energy* 2008; **11**: 685–702, doi:10.1002/we.302.

[4] Böttcher F, Renner C, Waldl HP, Peinke J: On the statistics of wind gusts. *Boundary-Layer Meteorology* 2003; **108**: 163–173.

[5] Böttcher F, Barth S, Peinke J: Small and large scale fluctuations in atmospheric wind speeds. *Stoch Environ Res Ris Assess* 2007; **21**: 299–308.

[6] Vindel J, Yague C, Redondo JM: Structure function analysis and intermittency in the atmospheric boundary layer. *Nonlinear Processes in Geophysics* 2008; **15**: 915–929.

[7] Research platform FINO I. URL http://www.fino-offshore.com/.

[8] Burton T, Sharpe D, Jenkinks N, Bossanyi E: *Wind Energy Handbook*. Wiley, 2001.

[9] Stull RB: *An Introduction to Boundary Layer Meteorology*. Kluwer Academic Publishers, 1994.

[10] Lovejoy S, Schertzer D, Stanway JD: Direct evidence of multifractal atmospheric cascades from planetary scales down to 1 km. *Physical Review Letters* 2001; **86**: 5200–5203.

[11] Hansen KS, Larsen GC: Characterising turbulence intensity for fatigue load analysis of wind turbines. *Wind Engineering* 2005; **29**: 319–329.

[12] Türk M, Emeis S: The dependence of offshore turbulence intensity on wind speed. *DEWI Magazine* 2007; **30**: 10–13.

[13] Panofsky H, Dutton JA: *Atmospheric Turbulence - Models and Methods for Engineering Applications.* Wiley, New York, 1984.

[14] Larsen G, Hansen K: The statistical distribution of turbulence driven velocity extremes in the atmospheric boundary layer – Cartwright/Longuet-Higgins revised. In Peinke J, Schaumann P, Barth S (editors), *Wind Energy. Proceedings of the Euromech Colloquium EUROMECH Colloquium 464b, Oldenburg (DE), 4–7 October 2005*, Springer, Berlin, 111–114.

[15] Castaing B, Gagne Y, Hopfinger EJ: Velocity probability density functions of high reynolds number turbulence. *Physica D* 1990; **46**: 177–200, doi:http://dx.doi.org/10.1016/0167-2789(90)90035-N.

[16] Morales A, Waechter M, Peinke J: Superstatistics of wind speed fluctuations. In *Accepted for Torque 2010, Heraklion, Greece*.

[17] Press WH, Teukolsky SA, Vetterling WT, Flannery BP: *Numerical Recipes in C The Art of Scientific Computing*. Cambridge University Press, second edition, 1996.

[18] Nielsen M, Larsen G, Mann J, Ott S, Hansen K, Pedersen B: Wind simulation for extreme and fatigue loads. Technical Report Riso-R-1437(EN), Risø DTU, 2003.

[19] Frisch U: *Turbulence: the legacy of A. N. Kolmogorov*. Cambridge University Press, 2001.

[20] Beck C: Superstatistics in hydrodynamic turbulence. *Physica D* 2004; **193**: 195–207.

[21] Kelley N, Jonkman B: Nwtc design codes. URL http://wind.nrel.gov/designcodes/preprocessors/turbsim/.

[22] Nawroth AP, Peinke J: Multiscale reconstruction of time series. *Phys. Lett. A* 2006; **360**: 234–237, doi:10.1016/j.physleta.2006.08.024.

[23] IEC: Wind Turbine Generator Systems, Part 12: Wind turbine power performance testing. International Standard 61400-12, International Electrotechnical Commission, 1998.

[24] Mücke T, Kleinhans D, Peinke J: Influence of small scale wind velocity fluctuations on the aerodynamic alternating loads. In *Proceedings of EWEC 2009*, Marseille.

Chapter 1

Introduction

1.1 Why a stochastic description of wind energy systems?

1.1.1 Atmospheric turbulence in the context of wind energy

Wind turbines are designed to extract energy from winds [1]. Atmospheric wind could be (arguably) seen as one of the most complex natural phenomena. This work does not attempt to describe the wind, but rather how wind installations react to it. Yet a proper description of any wind energy system implies having a basic understanding of its driving force. Atmospheric wind (on planet Earth) is a product of the unevenly-distributed solar radiation, that mostly heats regions close to the equator. Coupled with temperature gradients between altitudes (the air is warmer close to the ground during day), large-scale convection cells that circulate the air through latitudes appear. Pressure gradients emerge that create a net force between air masses. These dynamics are coupled with the Coriolis effect as a result of the Earth's surface being a non-inertial, rotating frame of reference. This simplified approach describes the prevailing wind patterns around the globe, that are called geostrophic winds. Additionally, local effects involving e.g. land masses and water masses have a strong impact on local wind situations. Wind conditions are historically measured and documented in a wind atlas that records the statistics of wind speed and direction in a region. This information is essential in order to select the best locations of future wind installations.

Wind turbines reach a typical height of $100 - 200$m. At such low altitudes[a], they operate in the turbulent boundary layer of the atmosphere [2]. The friction of the air on the Earth's surface generates a vertical shear, and the air velocity is zero at the ground and non-zero above. Additional forcing is also induced by local variations of temperature, humidity, orography, etc. This results in a largely turbulent flow close to the ground [3]. The physics of these *outdoor* effects combine to the staggeringly difficult physics of turbulence [4]. A simplification is used historically, based on observations of Van der Hoven in 1957 [5][b]. He introduced the concept of a spectral gap as a range of spectral frequencies where wind dynamics would appear to have less energy. This gap would separate the geostrophic dynamics (that occur at scales of hours and longer) from turbulence (for scales of minutes and less). Under this hypothesis, the

[a] An upper boundary for the atmosphere is commonly defined as the Kármán line at 100km, above which the air becomes too thin to support aeronautic flights.

[b] It is interesting to note that this apparently essential concept was not overly debated [6].

two regimes would be clearly separated and could be described separately[c]. The validity of this approach remains an open physical question. More recently, some multifractal approaches were developed to extend existing models of homogeneous isotropic turbulence to its atmospheric counterpart, as e.g. proposed by Refs. [3, 4, 9, 10, 11, 12, 13, 14, 15, 16, 17]. Nevertheless, fast wind fluctuations (of minutes and less) are the product of 3D turbulence. This justifies a description of wind turbulence, and its impact on wind energy systems.

1.1.2 The complex nature of fluid motion

A fluid flow is a physical system composed of many moving molecules that interact with each other to some degree. The velocity $\mathbf{u}(\mathbf{x},t)$ at position $\mathbf{x}$ and time t of a fluid continuum is described by Navier-Stokes equation, which is a special case of Newton's law of motion for fluids [7]

$$\begin{aligned} \partial_t u_i + u_j \partial_j u_i &= -\frac{1}{\rho}\partial_i p + \nu \partial_{jj} u_i + F_i \\ \partial_t \rho &= -\partial_j(\rho u_j) \end{aligned} \tag{1.1}$$

with $u_i(\mathbf{x},t)$ the component of $\mathbf{u}$ along the spatial axis x_i. $p(\mathbf{x},t)$ is the pressure of the fluid, $\rho(\mathbf{x},t)$ its density, ν its kinematic viscosity, and $\mathbf{F}(\mathbf{x},t)$ is the sum of all external forces acting on the system. One should note that $\partial_t = \frac{\partial}{\partial t}$, $\partial_j = \frac{\partial}{\partial x_j}$ and $\partial_{ij} = \frac{\partial^2}{\partial x_i \partial x_j}$. This partial differential equation has not been solved algebraically yet, owing to its very complex mathematical nature[de]. A well-known property of such dynamical system is chaos, where the system is so sensitive to initial conditions that a prediction of its future evolution is very limited[f]. Computational Fluid Dynamics (CFD) methods are commonly used to solve Navier-Stokes equation numerically. In most human-sized applications, and especially when the fluid is air, chaotic turbulent dynamics are present. Because of the strong non-linearity of turbulent regimes, one cannot use a superposition principle easily[g]. For a turbulent flow, dynamics are observed on

[c]It should be noted that geostrophic wind is typically considered as a two-dimensional flow. On the contrary, microscale turbulence is three-dimensional [7]. 2D and 3D turbulence are fundamentally different. In order to understand this, one should note that energy dissipation mostly occurs at microscales due to viscous friction. In 3D flows, energy is transported from large to small scales until it is dissipated at some small, viscous scale. On the contrary, for 2D flows the energy is transported towards large coherent structures that are dissipated very slowly, see e.g. [8] for a statistical description. This has the consequence that 3D flows fluctuate much more than 2D flows, that could be seen as quasi-stationary.

[d]Ref. [18] describes the three *N's* properties of Navier-Stokes equation that render the problem of turbulence as "impossibly difficult". First, the nonlinear property resulting from the nonlinear term $u_j \partial_j u_i$ can give raise to chaotic behavior. Second, this equation is nonintegrable. Third, the pressure term is nonlocal, that is, it depends in each spatial point on the velocity in the entire domain.

[e]As of today, few non-linear systems have known algebraic solutions. Numerical solvers have been developed in the past decades to make use of the increasing computing power available, but remain limited for many real-life applications. Besides trying to solve nonlinear equations numerically [19], theoretical considerations for the existence, stability or bifurcation of potential solutions are of interest to classify nonlinear dynamical systems [20].

[f]It should be noted that a chaotic system can be deterministic. In this case, the future state of the system is fully determined by its present state. However, a tiny variation in the present state can lead to a large deviation of the future states. This is the case of e.g. weather models, that must be regularly readjusted to the actual weather conditions in order to properly predict the weather in the near future.

[g]A Reynolds decomposition can be done to split the wind speed $u_i(\mathbf{r},t)$ into its mean, time-averaged part $\bar{u_i}(\mathbf{r})$ plus some fluctuations $u_i{}'(\mathbf{r},t)$. A Reynolds-averaged Navier-Stokes (RANS) equation then arises for the mean

a large range of spatio-temporal scales. For a proper description, even of the macroscopic behavior, the system must be described at all smaller scales (ideally until Taylor microscale λ, where viscous forces dampen the fluctuations). This makes the problem extremely demanding numerically, because of the large separation between the large size of the macroscopic domain and the microscales that should be resolved. This is particularly true for large 3D domains, as the spatial size of the model box must be limited to maintain reasonable calculation times. Defined as the ratio of inertial to viscous forces, the Reynolds number *Re* is a good measure of the computational cost. At low Reynolds numbers, viscous forces dominate at all scales and fluctuations are rapidly damped, giving a smooth, laminar flow that can be modeled easily. At high Reynolds numbers, inertial forces dominate the flow that can develop to become turbulent.

An alternative approach consists in doing a statistical description of the system, rather than trying to solve all its degrees of freedom. In such methods, the microscopic information is described through statistical estimates, and the focus lies on the macroscopic properties of the system as a whole. One can define a velocity increment $\mathbf{u}(\mathbf{x}+\mathbf{r},t)-\mathbf{u}(\mathbf{x},t)$ as the velocity difference over a spatial scale (i.e. distance) $r = ||\mathbf{r}||$ [7]. The work of Kolmogorov in 1941 [21, 22, 23] encouraged a statistical description of such velocity increments[h]. The approach builds upon the work of Richardson in 1922 [24], who introduced the concept of cascade. In this paradigm, energy (typically motion) contained at some scale r cascades down *ad infinitum* towards smaller scales. This justifies a study of the properties of turbulent flows at various scales r, giving raise to a new school of turbulence. Kolmogorov brought refinements in 1962 [25] that included the effect of viscosity at small molecular scales[i]. This summarizes the concept of a turbulent cascade (for a 3D flow), where the kinetic energy present in some large spatial structure distributes itself within smaller and smaller structures (vortices), until it reaches a small viscous scale where molecular friction converts it into heat. These scale dynamics motivated the creation of mathematical concepts such as scale invariant, fractal, or multiplicative processes, whose statistical properties are studied in scales (rather than in time or space) [26, 27, 28, 29, 30]. The scaling properties of turbulence remain actively studied [31, 32, 33, 34, 35, 36, 37, 38], and constitute one of the many active fields of turbulence research.

1.1.3 Stochastic approach to complexity: a historical example

Brownian motion is a famous historical case that exemplifies the stochastic description of a complex dynamical system. It was observed in 1827 by the botanist Robert Brown as the motion of a macroscopic particle immersed in (or suspended on) a viscous fluid, that is composed of many microscopic elements. A complete description of the problem would imply to describe the motion of each microscopic element in the fluid, and their interaction with the macroscopic particle. Besides being practically inaccessible, the very many microscopic information of the system is usually not needed. This information would depend strongly on the initial conditions, and would not be a reproducible experiment.

flow $\bar{u}_i(\mathbf{r})$, but in this case an additional Reynolds stress tensor appears. The task of properly describing this stress is an active research topic, for which turbulence models are specifically developed.

[h] It should be noted that Kolmogorov's work in 1941 addresses flows in the limit of very large Reynolds numbers, where viscous effects are inexistent.

[i] One should note that the development of this theory was brought about by the contributions of many scientists, and not only by Kolmogorov.

Instead, a probabilistic description was introduced in respectively 1905 and 1906 by Einstein [39] and Schmoluchowski for the motion of the macroscopic particle of mass m. In 1906, Langevin proposed a simple approach to describe its motion [40]. Given that the particle moves with a velocity v, one can introduce a deterministic drag force $F_d = -kv$ that accounts for the viscosity of the fluid. Additionally, if the mass m is small enough, the particle will be partly driven by the thermal fluctuations within the fluid. At this point, a fluctuating, *stochastic* force $F_s(t)$ is introduced to describe statistically all the random collisions of the particle with the microscopic elements[j]. The particle motion can be modeled following

$$m\dot{v} = F_d(t) + F_s(t) = -kv + F_s(t)\,. \tag{1.2}$$

Rewriting the stochastic force $F_s(t) = m \cdot \Gamma(t)$, one can define the so-called Langevin force $\Gamma(t)$. Equation 1.2 becomes

$$\dot{v} = -\alpha v + \Gamma(t) \tag{1.3}$$

with $\alpha = k/m$ a relaxation coefficient. Some information on Γ is necessary at this point. $\langle\Gamma(t)\rangle = 0$ because the average behavior of the particle is described as $\langle\dot{v}\rangle = \langle-\alpha v\rangle$ [41]. Another way to address this is to say that collisions coming from one side are equally probable as those coming from the other side, giving for the probability density $f(\Gamma)$ the symmetry $f(\Gamma) = f(-\Gamma)$, confirming $\langle\Gamma(t)\rangle = 0$. Additionally, collisions are considered as independent events, that occur during a very short time. This collision time is much shorter than the typical reaction time $1/\alpha$ of the mass m, so that collisions at an instant are independent of those at an instant later, as proposed by Einstein in [39]. This implies that the stochastic force is uncorrelated, i.e., $\langle\Gamma(t)\Gamma(t')\rangle = q\delta(t-t')$, where q is a measure of thermal diffusivity [k]. To summarize,

$$\begin{cases} \big\langle\Gamma(t)\big\rangle = 0 \\ \big\langle\Gamma(t)\Gamma(t')\big\rangle = q\delta(t-t')\,. \end{cases} \tag{1.4}$$

Brownian motion serves as a historical introduction to the more general class of Langevin processes, which are presented in greater detail in section 1.2.4. Similar approaches were developed to adapt the flexible structure of stochastic processes to real-life applications, such as e.g. homogeneous isotropic turbulence [43, 44, 45, 46, 47, 48, 49, 50, 51, 52, 53, 54], atmospheric wind [55, 56, 57, 58], the description of rough surfaces [59, 60, 61, 62, 63], cardiology [64], geoscience [65], electrical systems [66], cosmic background radiation [67] or complex networks [68]. The example of turbulent aerodynamics is introduced in section 1.1.4.

1.1.4 Stochastic approach to complexity: the example of turbulent aerodynamics

The aerodynamic force acting on a wind turbine airfoil represents a good example of an object reacting to a turbulent forcing. This problem can be addressed experimentally by performing

[j] While the collisions of fluid elements with the particle are fully deterministic in a mechanical sense, they appear as random when studying only the macroscopic properties of the system. This simplification of the many degrees of freedom into few macroscopic variables is the essence of stochastic theory. It describes the overwhelmingly numerous interactions through a probabilistic description of the macroscopic variables of the system.

[k] Ref. [41] shows that $q = 2\alpha K_B T/m$ for a fluid at temperature T. K_B is Boltzmann constant, see Ref. [42] for an introduction to thermodynamics.

a wind tunnel measurement, see e.g. Ref. [69]. Also, CFD methods are commonly used in this case, see e.g. Ref. [70], but they are very demanding for several reasons. The flow is air, and has typically a low viscosity $\nu \simeq 1.5 \cdot 10^{-5}\text{m}^2/\text{s}$. A complete model of a flow around a commercial wind turbine implies to model a large box of typically $L \sim 100\text{m}$. The wind velocity is in the order $u \sim 10\text{m/s}$, yielding a Reynolds numbers $Re = uL/\nu \sim 10^8$.[1] Such large Reynolds numbers correspond to largely turbulent flows [7]. The numerical effort to solve Navier-Stokes equation numerically is proportional to Re^3 for a three-dimensional flow.

Yet in many applications, it is unnecessary to have detailed information about the flow structure. Sometimes a statistical description of the motion of an object within that flow is of interest. In such a case, one could address the problem following Langevin's approach to Brownian motion. Instead of trying to resolve the many microscopic degrees of freedom of the flow ($\sim Re^3$), one can describe the aerodynamic forces acting on the object. We consider here the example of an airfoil placed within a turbulent airflow in a wind tunnel at $Re = 7 \cdot 10^5$, as documented in Ref. [69]. A statistical description of the airfoil lift and drag forces is of interest to describe the behavior of the airfoil, see equation (1.62) in section 1.C. The lift coefficient $C_L(t)$ and its histogram are presented in figure 1.1. Similarly to equation (1.3) for Brownian

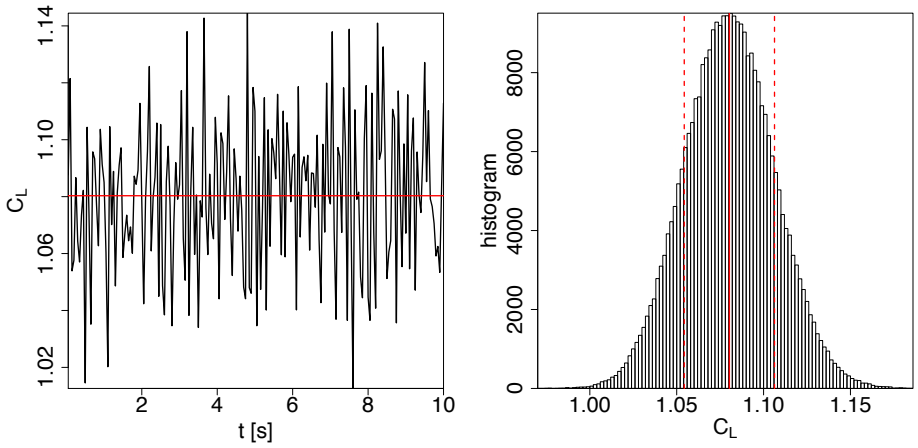

Figure 1.1: (a) Excerpt of lift coefficient $C_L(t)$ measured in wind tunnel for an angle of attack $\alpha = 8^o$. The signal was dowmsampled to 20Hz to filter the fastest dynamics; (b) histogram of C_L. The average value $\bar{C_L}$ (red line) and standard deviation σ_{C_L} (red dashed lines) are represented.

motion, one can propose a simple stochastic model for $C_L(t)$ following

$$\dot{C_L}(t) = -\alpha\big(C_L(t) - \bar{C_L}\big) + \Gamma(t) \tag{1.5}$$

with $\alpha \simeq -14.65/\text{s}$ (can be estimated using equation (1.19)). Γ is close to the theoretical case in equation (1.4) with $q \simeq 0.02/\text{s}$. While this stochastic model does not reproduce all statistical features observed on measured data, one-point statistics (and to some extent some two-point statistics) match that of the measurement. This illustrates how a simple stochastic approach can be used to model the macroscopic behavior of an a priori complex aerodynamic system

[1] Similar Reynolds values are observed when modeling the flow around a rotor blade section, as $L \sim 10\text{m}$ and $u \sim 10 - 100\text{m/s}$ for the effective wind velocity relative to the rotor blades, see equation (1.63).

without going into the details of the many microscopic interactions. More refined stochastic models of aerodynamic forces are presented in e.g. [71, 72]. The central focus of this work is the description of some complex, wind-driven systems in terms of simple stochastic models.

1.2 Introduction to stochastic theory

Section 1.1 introduced the notion of a complex system, where many microscopic interactions contribute to some random-like dynamics of macroscopic estimates. Let us consider a one-dimensional[a] dynamical system described by the variable $x(t)$. The process $x(t)$ is defined as *stochastic* because its time evolution is described in a probabilistic sense[b]. Although the sample path $x(t)$ can be continuous (and should be for a purely Markov process [40]), practical applications mostly involve discrete signals. From the continuous process $x(t)$, only N samples x_1, x_2, ..., x_N are known at discrete times $t_1 < t_2 < ... < t_N$. $x(t_i) = x_i$ and $x(t_{i+1}) = x_{i+1}$ are known, yet x(t) for $t_i < t < t_{i+1}$ is unknown. The dynamical system is then described by the discrete samples x_i, so that a complete (statistical) description is given through the joint probability distribution

$$f(x_N,t_N;x_{N-1},t_{N-1};...;x_1,t_1)\,, \tag{1.6}$$

where $f(A;B;C)$ is the probability of A and B and C happening. The value of sample x_i at time t_i is stochastic, but its probability to have a given value is fixed. Similarly, one can define the conditional probability p following

$$\begin{aligned} &f(x_N,t_N;x_{N-1},t_{N-1};...;x_1,t_1) \\ &\quad = p(x_N,t_N|x_{N-1},t_{N-1};...;x_1,t_1)\cdot f(x_{N-1},t_{N-1};...;x_1,t_1)\,, \end{aligned} \tag{1.7}$$

where $p(A|B;C)$ is the probability of A happening conditioned on (given) B and C happen.

The simplest stochastic process that can be thought of is a purely random process with independent samples x_i [41]. Independence implies that $p(x_i,t_i|Y) = f(x_i,t_i)$ for any arbitrary condition Y, that is, no matter what the condition Y is, x_i will not depend on it. As a consequence, the joint probability of an independent process is

$$f(x_N,t_N;x_{N-1},t_{N-1};...;x_1,t_1) = \prod_{i=1}^{N} f(x_i,t_i)\,. \tag{1.8}$$

1.2.1 Markov property

Besides the trivial case of an independent process, the next simplest process is a Markov process [41]. For a Markov process, only information about the present state is necessary to describe

[a] Only an account of one-dimensional stochastic systems is given here, as it suffices for the problem at hand. However, a multi-dimensional description of stochastic systems is possible, as presented in Ref. [41].

[b] Under some weak conditions (that are not presented here for the sake of brevity), if one would let several realizations $x_a(t)$, $x_b(t)$, ..., $x_z(t)$ of that process x evolve in time, one would see that at a given future time t', the exact values of the process have a random character, i.e. , $x_a(t') \neq x_b(t') \neq ... \neq x_z(t')$. Yet the probability to obtain a given value remain fixed, giving for the probability distribution $f(x_a,t') = f(x_b,t') = ... = f(x_z,t')$.

the next future state, regardless of the past state. This means that the state of system x_i at time t_i depends on x_{i-1} at time t_{i-1}, and the conditional probability can be simplified following

$$p(x_i,t_i|x_{i-1},t_{i-1};...;x_1,t_1) = p(x_i,t_i|x_{i-1},t_{i-1})\,. \tag{1.9}$$

Equation (1.7) can be rewritten for a Markov process as

$$f(x_N,t_N;x_{N-1},t_{N-1};...;x_1,t_1) = f(x_1,t_1)\prod_{i=2}^{N} p(x_i,t_i|x_{i-1},t_{i-1})\,. \tag{1.10}$$

The Markov property is often described as *memoryless*. One should note that a (one-dimensional) Markov process $x(t)$ cannot describe n-order differential systems with $n > 1$[c]. In some cases, the Markov property can emerge by introducing new variables (which remain to be found) to a non-Markov dynamical system, i.e., by making it higher-dimensional.

The total probability theorem gives [73]

$$f(x_i,t_i) = \int dx_{i-1}\, f(x_i,t_i;x_{i-1},t_{i-1})\,. \tag{1.11}$$

Similarly for the conditional probability

$$\begin{aligned} p(x_i,t_i|x_{i-2},t_{i-2}) &= \int dx_{i-1}\, p(x_i,t_i;x_{i-1},t_{i-1}|x_{i-2},t_{i-2}) \\ &= \int dx_{i-1}\, p(x_i,t_i|x_{i-1},t_{i-1};x_{i-2},t_{i-2}) p(x_{i-1},t_{i-1}|x_{i-2},t_{i-2})\,. \end{aligned} \tag{1.12}$$

Using the Markov assumption in equation (1.9), equation (1.12) becomes the Chapman-Kolmogorov equation

$$p(x_i,t_i|x_{i-2},t_{i-2}) = \int dx_{i-1}\, p(x_i,t_i|x_{i-1},t_{i-1}) p(x_{i-1},t_{i-1}|x_{i-2},t_{i-2})\,. \tag{1.13}$$

For non-Markov processes, the future state does not depend only on the present state, but also on a number of past states, see also [41, 74, 75]. One can define the Einstein-Markov length τ_{mar} (further referred to as Markov length) as the length of the memory kernel, that is the number of past states that influence the present state. Einstein presents this coarse-graining as a necessary time interval such that the stochastic forces become independent events [39]. This implies the relation

$$p(x_i,t_i|x_{i-1},t_{i-1};...;x_1,t_1) = p(x_i,t_i|x_{i-1},t_{i-1};...;x_j,t_j) \tag{1.14}$$

with $t_j = t_i - \tau_{mar}$. Experimental signals usually exhibit a non-vanishing, yet finite Markov length, see e.g. [76, 77] for turbulence. Various Markov tests exist to search for a Markov length in data sets. Some tests are presented and applied in section 5.1 for various wind energy signals.

[c]Let us consider the example of a deterministic (a special case of stochastic) process $x(t)$ governed by an arbitrary second-order differential equation $\ddot{x} = F(x,\dot{x})$. $x(t)$ is not a Markov process because the future state $x(t+dt)$ does not depend only on the present state $x(t)$, but also on $\dot{x}(t)$. Knowing $x(t)$ does not suffice to know $x(t+dt)$. However, the two-dimensional process $\{x(t),\dot{x}(t)\}$ is a (two-dimensional) Markov process, so that knowing $\{x(t),\dot{x}(t)\}$ suffices to know $\{x(t+dt),\dot{x}(t+dt)\}$.

1.2.2 Kramers-Moyal expansion

The stochastic process $x(t)$ evolves probabilistically in time. Because of its partly random nature, it is inappropriate to describe its exact time evolution, which is not reproducible. Instead, a description of the probability $f(x,t)$ to find a value x at time t is relevant. For a Markov process, $f(x,t)$ follows a master equation

$$\frac{\partial f(x,t)}{\partial t} = \int dx' \left[w(x' \to x) f(x',t) - w(x \to x') f(x,t) \right], \tag{1.15}$$

where $w(a \to b)$ is the transition rate from state a to state b. More concretely, the law of total probability implies

$$\begin{aligned} f(x,t+\tau) &= \int dx' \, f(x,t+\tau;x',t) \\ &= \int dx' \, p(x,t+\tau|x',t) f(x',t) \end{aligned} \tag{1.16}$$

with $\tau \geq 0$.

Conditional moments are defined following [41]

$$\begin{aligned} M^{(n)}(x',t,\tau) &= \int dx \; (x-x')^n \, p(x,t+\tau|x',t) \\ &= \left\langle \left[x(t+\tau) - x(t) \right]^n \middle| x(t) = x' \right\rangle \end{aligned} \tag{1.17}$$

where $\langle A|B \rangle$ is defined as the mean value of A given that condition B is fulfilled. One can derive the Kramers-Moyal expansion (see complete derivation following Ref. [41] in appendix 1.A)

$$\frac{\partial f(x,t)}{\partial t} = \sum_{n=1}^{\infty} \left(-\frac{\partial}{\partial x} \right)^n D^{(n)}(x,t) f(x,t) \tag{1.18}$$

with the Kramers-Moyal coefficients defined as

$$\begin{aligned} D^{(n)}(x,t) &= \frac{1}{n!} \lim_{\tau \to 0} \frac{1}{\tau} M^{(n)}(x,t,\tau) \\ &= \frac{1}{n!} \lim_{\tau \to 0} \frac{1}{\tau} \left\langle \left[x(t+\tau) - x(t) \right]^n \middle| x(t) = x \right\rangle \\ &= \frac{1}{n!} \left. \frac{\partial M^{(n)}(x,t,\tau)}{\partial \tau} \right|_{\tau=0}, \end{aligned} \tag{1.19}$$

where the third relation owes to $M^{(n)}(x,t,\tau=0) = 0$.

The Kramers-Moyal expansion can be formally written

$$\frac{\partial f(x,t)}{\partial t} = L_{KM}(x,t) \, f(x,t) \tag{1.20}$$

with the Kramers-Moyal operator defined as

$$L_{KM}(x,t) = \sum_{n=1}^{\infty} \left(-\frac{\partial}{\partial x} \right)^n D^{(n)}(x,t) \,. \tag{1.21}$$

Ref. [41] *assumes*[d] that the Kramers-Moyal expansion describes a Markov process, as the evolution $\partial f(x,t)/\partial t$ of the process at time t depends only on its present state $f(x,t)$, and not on some past states $f(x,t')$ for $t' < t$.

One should note that some difficulties arise when estimating these coefficients from experimental data. Some optimized algorithms were proposed in Refs. [78, 79, 80, 81, 82, 83] to refine the estimation of Kramers-Moyal coefficients from experimental data. Refs. [84, 85, 86, 87, 88] address the finite-time effects that appear as one cannot reach the limit $\tau \to 0$ with experimental data, that has a finite sampling rate. Refs. [89, 90, 91, 92, 93, 84, 94, 95, 96] improve the estimation in the presence of measurement noise within experimental data. For processes with a finite Markov length τ_{mar} (either intrinsic or artificially added through experimental limitation), the Kramers-Moyal expansion can be generalized following

$$\frac{\partial f(x,t)}{\partial t} = \int_{t-\tau_{mar}}^{t} dt'\, L_{KM}(x,t')\, f(x,t')\,. \tag{1.22}$$

1.2.3 Fokker-Planck equation

The Fokker-Planck equation is a special case of the Kramers-Moyal expansion for which $D^{(n)}(x) = 0$ for $n \geq 3$. This relates to the Pawula theorem, which states[e] that the Kramers-Moyal expansion (1.18) either stops after $n = 1$, after $n = 2$, or require an infinity of terms, see [41]. This theorem shows from the generalized Schwartz inequality that $[M^{(2n+m)}]^2 \leq M^{(2n)} \cdot M^{(2n+2m)}$ for any set of integers $(n,m \geq 0)$. This implies that $D^{(n>2)} = 0$ if there exists one integer $r > 0$ such that $D^{(2r)} = 0$.

If a Markov process $x(t)$ satisfies the Pawula theorem, the Kramers-Moyal expansion stops after the second term and the probability distribution $f(x,t)$ is described by the Fokker-Planck equation

$$\begin{aligned}\frac{\partial f(x,t)}{\partial t} &= \left[-\frac{\partial}{\partial x} D^{(1)}(x,t) + \frac{\partial^2}{\partial x^2} D^{(2)}(x,t) \right] f(x,t) \\ &= L_{FP}(x,t)\, f(x,t)\,.\end{aligned} \tag{1.23}$$

The Fokker-Planck operator reads

$$L_{FP}(x,t) = -\frac{\partial}{\partial x} D^{(1)}(x,t) + \frac{\partial^2}{\partial x^2} D^{(2)}(x,t). \tag{1.24}$$

The stationary solution $f_{st}(x)$ of the Fokker-Planck equation (for time-independent coefficients $D^{(1,2)}(x)$) can be derived from

$$\frac{\partial f_{st}(x)}{\partial t} = \left[-\frac{\partial}{\partial x} D^{(1)}(x) + \frac{\partial^2}{\partial x^2} D^{(2)}(x) \right] f_{st}(x) = 0 \tag{1.25}$$

[d] Some criticism of the Kramers-Moyal expansion is formulated in Ref. [40], where it is argued that the Kramers-Moyal expansion cannot describe the evolution of some Markov jump processes, but only approximate it.

[e] The Pawula theorem only applies if the conditional probability $p(x,t+\tau|x',t)$ is a non-negative function.

that is solved by

$$f_{st}(x) = \frac{N}{D^{(2)}(x)} exp\left(\int^{x} \frac{D^{(1)}(x')}{D^{(2)}(x')} dx' \right) \tag{1.26}$$

with N a normalization constant such that $\int_{-\infty}^{\infty} f_{st}(x)dx = 1$.

Similarly, the Fokker-Planck equation exists for a conditional probability $p(x,t|x',t')$ (that is the distribution $f(x,t)$ for the initial condition $f(x,t') = \delta(x-x')$) and gives

$$\frac{\partial}{\partial t} p(x,t|x',t') = L_{FP}(x,t)\ p(x,t|x',t')\,, \tag{1.27}$$

which has a unique initial condition $p(x,t|x',t) = \delta(x-x')$.

If the process is stationary in time[f], $L_{FP}(x,t) = L_{FP}(x)$ and $D^{(n)}(x,t) = D^{(n)}(x)$, so equation (1.27) has a formal solution

$$p(x,t+\tau|x',t) = e^{\tau\, L_{FP}(x)} \delta(x-x') \tag{1.28}$$

owing to the initial condition $p(x,t|x',t) = \delta(x-x')$.

It is shown in Ref. [41] that equation (1.28) holds for a time-dependent $L_{FP}(x,t)$ if the time increment τ is sufficiently small so that $D^{(n)}$ can be seen as unchanged coefficients. Based on the definition of the delta function $\delta(x-x')$ (see equation (1.50) in appendix 1.A), equation (1.28) gives the short-time propagator of the Fokker-Planck equation for small τ (see derivation in equation (1.56) in appendix 1.A)

$$p(x,t+\tau|x',t) = \frac{1}{\sqrt{4\pi\tau D^{(2)}(x',t)}} exp\left(- \frac{[x-x'-\tau D^{(1)}(x',t)]^2}{4\tau D^{(2)}(x',t)} \right). \tag{1.29}$$

The Fokker-Planck equation is a linear partial differential equation that can be solved numerically. Besides the direct method that consists in numerically approximating the differential operators, one can use a path integral method [41]. Similarly to what is done in quantum mechanics to solve the Schrödinger equation, this method is easy to implement. Given an initial condition $f(x,t_0)$, equation (1.16) gives $f(x,t_0+\tau)$ using $p\big(x,t_0+\tau\big|x,t_0\big)$. This can be iterated $n-$times to calculate $f(x,t_n)$ from $f(x,t_{n-1})$ for time $t_n = t_0 + n\tau$. One can formulate this following

$$\begin{aligned} f(x,t_n) = \int dx_{n-1} \int dx_{n-2} ... \int dx_0 \\ p\big(x,t_n\big|x_{n-1},t_{n-1}\big)\, p\big(x_{n-1},t_{n-1}\big|x_{n-2},t_{n-2}\big) ... p\big(x_1,t_1\big|x_0,t_0\big) f(x_0,t_0)\,. \end{aligned} \tag{1.30}$$

For a small enough time increment τ, the conditional probability is given by equation (1.29). A similar approach can be used for $p(x,t_0+n\tau|x',t_0)$ using the Chapman-Kolmogorov equation (1.13) and the initial condition $p(x,t_0|x',t_0) = \delta(x-x')$.

[f] The process $x(t)$ is defined here as (time-) stationary if $f(x_N,t_N;...;x_1,t_1) = f(x_N,t_N+\tau;...;x_1,t_1+\tau)$ for an arbitrary time shift τ.

1.2.4 Langevin equation

Based on the historical example of Brownian motion, a Langevin equation for a *Langevin process* $x(t)$ reads

$$\frac{dx}{dt} = D^{(1)}(x,t) + \sqrt{D^{(2)}(x,t)} \cdot \Gamma(t)\,. \tag{1.31}$$

The Kramers-Moyal coefficients are the coefficients defined in equation (1.19) (see derivation in appendix 1.B).

The time evolution of a sample path $x(t)$ is described by so-called drift coefficient $D^{(1)}(x,t)$ and diffusion coefficient $D^{(2)}(x,t)$. In parallel, the probability $f(x,t)$ is described by the Fokker-Planck equation (1.23). For a given set of drift and diffusion coefficients, the Fokker-Planck equation gives a unique solution $f(x,t)$. On the contrary, the Langevin equation can generate different sample paths $x_i(t)$ that have different values (due to the randomness of the Langevin noise $\Gamma_i(t)$). Yet the probability that $x_i(t_j) = X$ is the unique solution of the Fokker-Planck equation $f(X,t_j)$.

The Langevin equation can be discretized following

$$\begin{aligned} x(t+dt) &= x(t) + \int_t^{t+dt} \frac{dx}{dt}(t')dt' \\ &= x(t) + \int_t^{t+dt} D^{(1)}(x,t')dt' + \int_t^{t+dt} \sqrt{D^{(2)}(x,t')}\Gamma(t')dt'\,. \end{aligned} \tag{1.32}$$

The integration of $\Gamma(t)$ is not defined mathematically, yet a physical interpretation of the stochastic integral is needed. The definition of stochastic integration in the sense of Itô gives[g]

$$\int_t^{t+dt} g(x,t')\Gamma(t')dt' = g(x,t) \int_t^{t+dt} \Gamma(t')dt'\,. \tag{1.33}$$

For $dt \ll 1$, $D^{(n)}$ can be taken as unchanged coefficients and equation (1.32) becomes

$$x(t+dt) = x(t) + D^{(1)}(x,t)dt + \sqrt{D^{(2)}(x,t)} \int_t^{t+dt} \Gamma(t')dt'\,. \tag{1.34}$$

The Langevin noise $\Gamma(t)$ fluctuates much faster than the stochastic process $x(t)$ and has a correlation length much shorter than dt (its theoretical correlation length is zero). The Langevin

[g] Another common approach to carry out a stochastic integral is the Stratanovich definition that reads $\int_t^{t+dt} g(x,t')\Gamma(t')dt' = g\left(\frac{x(t+dt)-x(t)}{2}\,,\, t+dt/2\right) \int_t^{t+dt} \Gamma(t')dt'$. The Stratanovich approach is more intuitive because it considers the value of the function g at the middle point of the integration range. Only the Itô interpretation is used here, as it is easier to implement numerically. Also, the definition of the Kramers-Moyal coefficients is different in the Stratanovich interpretation. Both interpretations are equivalent, as they yield identical probability distributions [97]. Ref. [98] summarizes various interpretations of the Langevin equation in the presence of non-constant $D^{(2)}$.

noise is related to a Wiener process $W(t)$ in that $\dot{W} = \Gamma(t)$, bringing the Stieltjes integral

$$\int_t^{t+dt} \Gamma(t')dt' = \int_t^{t+dt} dW(t') = \sqrt{dt} \cdot \eta(t) \tag{1.35}$$

with $\eta(t)$ a set of independent, Gaussian-distributed samples following $\langle \eta(t) \rangle = 0$ and $\langle \eta(t)^2 \rangle = 2$. The discrete form of the Langevin equation for a small time increment dt becomes

$$x(t+dt) = x(t) + D^{(1)}(x,t)dt + \sqrt{D^{(2)}(x,t)dt} \cdot \eta(t)\,. \tag{1.36}$$

A sample path $x(t_0 + n.dt)$ can be generated by iterating $n-$times the integration from an initial condition $x(t_0)$.

1.3 Introduction to wind energy systems[h]

1.3.1 Physical limitations to the extraction of wind power

The concept of power performance is introduced here for wind turbines. While only horizontal-axis three-bladed electrical wind turbines are considered here, most findings apply to other wind energy designs. In this section, a simplified understanding of fluid mechanics is applied to wind turbines. The complexity of turbulence is first set aside, so as to understand the fundamental behavior of a wind turbine in a uniform flow at steady-state. The impact of a realistic turbulent flow on a wind turbine is studied in later sections.

As a wind turbine converts the power from the wind P_{wind} into available electrical power denoted with P, one can assume the following relation

$$P(u) = c_P(u) \cdot P_{wind}(u)\,, \tag{1.37}$$

where u is the wind speed through the wind turbine and $c_P(u)$ the so-called power coefficient which represents the efficiency of the machine. As the input $P_{wind}(u)$ cannot be controlled, improving power performance means increasing the power coefficient $c_P(u)$. The power contained in a laminar incompressible flow of mass $m = \rho V = \rho A x$ and density ρ moving along the $x-axis$ with constant (upstream) speed u through a vertical plane of area A is

$$P_{wind}(u) = \frac{d}{dt}E_{kin} = \frac{d}{dt}\left(\frac{1}{2}mu^2\right) = \frac{1}{2}\rho A u^3\,. \tag{1.38}$$

Let us consider a mass of air moving towards a wind turbine, which can be represented by an actuator disc[a] of radius R. When crossing the wind turbine, the wind is affected as parts of its

[h] This section is a summary of a book chapter that has been accepted, and is being published as PATRICK MILAN, MATTHIAS WÄCHTER and JOACHIM PEINKE: Wind Turbine Power Performance and Application to Monitoring, in *Handbook of Wind Power Systems (HWPS): Optimization, Modeling, Simulation and Economic Aspects*, editors S. Rebennack, P. M. Pardalos, V. Pappu, M. V. Pereira and N. A. Illiadis, publisher Springer, 2013.

[a] An actuator disc is an infinitely thin disc through which the air can flow without resistance, as proposed by Froude and Rankine's momentum theory.

energy is extracted. Introducing the downstream wind velocity u_{down}, this extraction of kinetic energy results in a drop in the wind speed from upstream to downstream, i.e., $u_{down} < u$.

The wind power cannot be totally converted into mechanical power because the wind turbine continuously takes energy out of the wind flow, which reduces its velocity. However, the flow needs to *escape* the wind turbine downstream with a speed $u_{down} > 0$. If all the power content of the wind would be extracted, the wind speed downstream would then become zero. As a consequence, the air would *accumulate* downstream and block newer air from flowing through the wind turbine through increasing pressure gradients, so that no more power could be extracted. This means that the wind flow must keep some energy to escape, which naturally sets a limit for the efficiency of any wind power system, and $c_P(u) < 1$. An optimal ratio of wind speeds $\mu = u_{down}/u$ can be found that allows for the highest energy extraction. Conservation of mass implies that the theoretical power coefficient is [1]

$$c_P(\mu) = \frac{1}{2}(1 + \mu - \mu^2 - \mu^3) \tag{1.39}$$

that has a maximum for $\mu_{max} = 1/3$, corresponding to a performance $c_P(\mu_{max}) = 16/27 \approx 0.593$. This limit is called the Betz limit, as it was found by Albert Betz in 1927 [99]. In other words, a wind turbine can extract at most a ratio $16/27$ of the power contained in the wind. This can be obtained when the wind speed downstream is one-third of the wind speed upstream, and two-thirds at the plane of the rotor. Betz' momentum theory only considers the mechanical transfer of energy from the wind to the rotor blades. The next step of the conversion from mechanical to electrical energy is not taken into account, as well as all energy losses. The more complex design of wind turbines causes lower values of c_P, typically $c_P < 0.5$. Also, criticism of Betz theory is given in [100, 101], leading to a less well defined upper limit of c_P. Additional considerations, e.g. the finite number of blades and losses due to the drag and stall effects on the blades are discussed in [1, 102].

A widely used representation of power performance is given by the relation of c_P to the tip speed ratio $\lambda = \frac{\omega R}{u}$, where ω is the rotational frequency of the rotor. λ is the ratio of the rotational speed at the tip of the blades to the upstream wind speed u. The dimensionless $c_P(\lambda)$ curve is introduced in figure 1.2 when considering three major sources of power loss:

- Following Newton's third law, the rotational motion of the rotor transfers angular momentum to the air flow downstream. This so-called *bouncing* loss is more important for slow rotating wind turbines (λ small) following equation (1.66) in appendix 1.C. For a small rotational velocity ωr, a larger rotational force F_r is required to obtain the same power, that transfers more angular momentum.

- Another important source of energy loss is the quality of the airfoil profile, whose imperfections increase the drag force. Profile losses mainly affect fast rotating machines, such that the lift-to-drag ratio C_L/C_D must be optimized for fast rotating turbines, see equation (1.69) in appendix 1.C. Furthermore the losses increase with the radius, such that the manufacturing quality of the blade tips is of primary importance for power performance.

- A good quality of the blade tips means especially that they should be as narrow as possible because this corresponds to an ideal airfoil with length infinity ($length/depth \to \infty$). With real blades there is always a flow around the end of the blade (forming an eddy

that is advected by the flow) from the high pressure area to the low pressure area. This partly levels the pressure difference and consequently reduces the lift force. Tip losses are reduced by fast rotation or an increased number of blades.

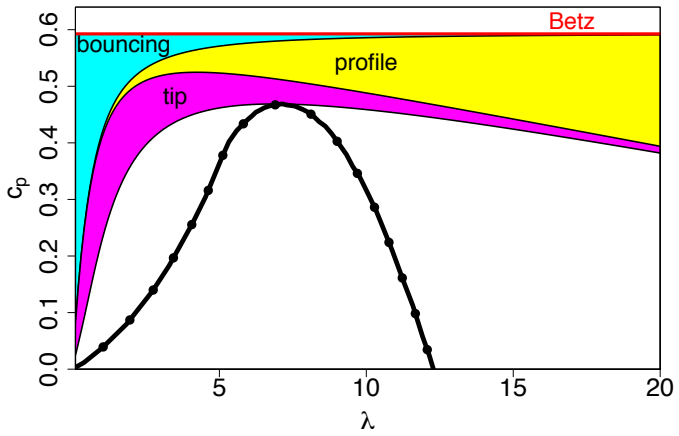

Figure 1.2: Typical $c_P(\lambda)$ curve (black dotted line). Betz limit (red line), the bouncing, profile and tip losses are illustrated. These results were obtained with a lift to drag ratio $C_L/C_D = 60$ and $z = 3$ blades. Maximum performance $c_P \simeq 0.475$ is obtained at $\lambda \simeq 7$, as typically used for three-bladed, power-generating wind turbines.

1.3.2 Basic wind turbine operation

Modern designs typically involve a regulation of the power output through changes both in the rotational frequency of the generator and in the pitch angle of each blade[b]. In order to reach optimal performance, the rotational frequency of the generator ω_g must be physically linked to the wind speed u. Additionally, the pitch angle β of the blades can be controlled to radically change the aerodynamic forces acting on the blades, see figure 1.7. The power production can be reduced by active pitch-to-feather (reduce angle of attack) of pitch-to-stall[c] strategies. Additional considerations such as mechanical loads or power stability are partly taken into account as well, see Ref. [102].

Modern variable-speed pitch-controlled wind turbines have four distinct modes of operation that are adapted to the wind speed:

- for $u \leq u_{cut-in}$,[d] the power contained in the wind is not sufficient to maintain the wind turbine into motion, and no power is produced;

[b] Other wind turbine designs involve fixed rotational frequency (called fixed-speed wind turbines) or fixed pitch angle (called fixed-pitch wind turbines). A more detailed description of control strategies is given in Ref. [102].

[c] Stall effects are obtained when the angle of attack of an airfoil exceeds a critical value, resulting in a sudden reduction in the lift force generated. A detailed study on airfoil lift effects can be found in [71].

[d] u_{cut-in} represents the minimum wind speed such that the wind turbine can extract power, typically in the order of $3-4m/s$.

- in partial load $u_{cut-in} \leq u \leq u_r$,[e] the wind turbine works at its maximum power performance, i.e. c_P is maximized. This is achieved in most of this wind speed range by increasing the rotational frequency ω as u increases so that the angle of attack α stays constant (see figure 1.7);

- in full load $u_r \leq u \leq u_{cut-out}$, [f] the wind turbine power output is limited to the rated power P_r. In this mode of operation, the pitch angle β is adjusted in real-time to maintain $P \approx P_r$;

- for $u > u_{cut-out}$ the pitch angle β is maximized to the feathered position so as to eliminate the lift forces on the blades. A braking device can be used in addition to block the rotation for safety reasons. As a consequence, the power production is stopped.

Along with the $c_P(\lambda)$ curve, a standard representation of a wind turbine power performance is given by a so-called power curve. The power curve gives the relation between the simultaneous wind speed u and electrical power output P (or mechanical in case of wind mills). An illustration of the theoretical curves $c_P(u)$ and $P(u)$ is given in Fig. 1.3 for the ideal case where no power losses are considered.

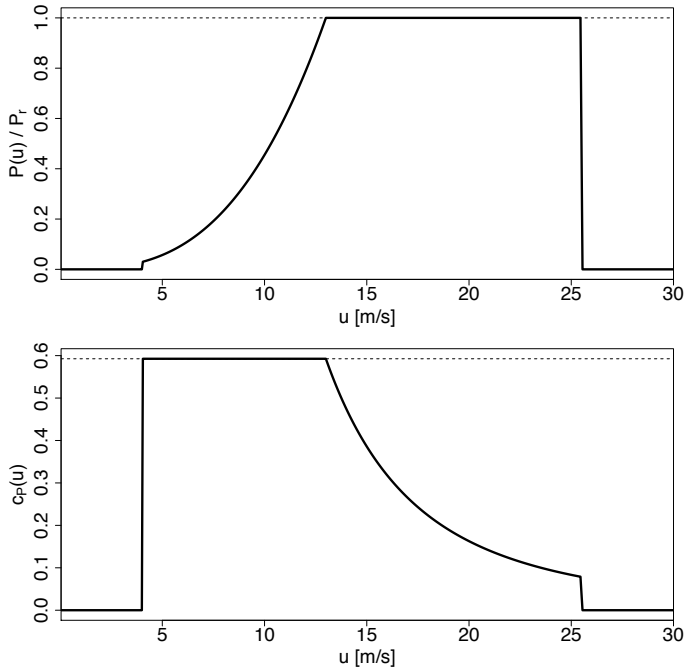

Figure 1.3: (upper) theoretical power curve $P(u)$. The rated power P_r is indicated (dashed line); (lower) theoretical power coefficient $c_P(u)$ for a variable-speed, variable-pitch wind turbine with $u_{cut-in} = 4$m/s, $u_r = 13$m/s and $u_{cut-out} = 25$m/s. Betz limit is indicated (dashed line).

[e] the rated wind speed u_r represents the minimal wind speed at which the wind turbine extracts the rated, maximum allowed power P_r, typically in the order of $11-14m/s$.

[f] $u_{cut-out}$ represents the maximum wind speed at which the wind turbine can safely extract power, typically in the order of $25-35m/s$.

Such theoretical strategy is only valid in the unrealistic case of a laminar inflow. Due to its size, in the order of 100m, a commercial wind turbine operates within flows at a Reynolds number in the order of $Re \sim 10^8$. Such high Reynolds-number flows are largely turbulent for relevant spatio-temporal scales. Also, the proximity of the rotor to the ground (the boundary layer of atmospheric flows) induces boundary-layer turbulence. Atmospheric wind measurements have turbulence intensities[g] of up to 30%, that correspond to strongly fluctuating inflows. Also, homogeneity is not valid[h] as spatial fluctuations are observed. Additionally, wind turbines render the turbulent inflow more complex, especially in the wake, see [103]. All these effects add up to a highly complex system, whose overall description is typically simplified to a statistical problem. The impact of turbulence on power performance is a widely studied topic in wind energy, see e.g. [104, 105, 106, 107, 108].

1.3.3 IEC power curve standard

The standard procedure to determine the power performance for wind turbines was defined by the International Electrotechnical Commission in 2005 in the norm IEC 61400-12-1 [109]. In a recent revision, norm IEC 61400-12-2 [110] includes nacelle anemometry as a valid wind measurement method for power curve estimation. The IEC procedure provides a unique methodology to ensure accuracy, consistency and reproducibility in the measurement and in the analysis of power performance. It consists first: of the minimum requirements for a power performance test and second: of a procedure to process the measured data without extensive knowledge. Only a brief overview is presented here.

First, measurements of wind speed u and power output P must be collected at a sampling frequency of 1Hz on a wind turbine operating under normal conditions. P is the net electrical power output fed to the grid, after all possible losses. u is measured at a fixed location[i] at hub height (on a met mast following Ref. [109] or on the turbine nacelle following Ref. [110]). Additionally, air temperature and pressure must be collected so as to estimate the air density. This allows to normalize either the wind speed or the power output (for resp. pitch-regulated or stall-regulated wind turbines) to a standard value of air density in order to obtain uniform results. Additionally the wind direction must be measured so as to reject directions where obstacles alter the wind inflow, including neighboring wind turbines.

Second, the measured data is processed. The data processing is mainly performed in two steps. After adequate normalization of the data, the first step consists in averaging the measured data over time intervals of 10 minutes. The IEC power curve is derived in a second step from the ten-minute averages using the so-called method of bins, i.e. the data is separated into wind speed intervals of width 0.5 m/s. In each interval i, bin averages of wind speed u_i and power

[g] The turbulence intensity $I = \sigma_u/\langle u \rangle$ is defined as the ratio of standard deviation σ_u to mean value $\langle u \rangle$ for the wind speed u for each ten-minute interval. It is a simple measure of the level of turbulence with respect to the mean flow.

[h] In the case of atmospheric flows close to the ground, homogeneity and isotropy are not even valid in a statistical sense, due to e.g. boundary layer effects.

[i] A measurement of wind speed at one point does not allow to estimate the spatial fluctuations acting on the rotor. Some research projects have used more advanced wind measurements of 1D profiles or 2D planes in front of wind turbines using e.g. LIDAR devices, see Ref. [111].

output P_i are calculated according to

$$u_i = \frac{1}{N_i}\sum_{j=1}^{N_i} u_{i,j} \quad , \quad P_i = \frac{1}{N_i}\sum_{j=1}^{N_i} P_{i,j} \tag{1.40}$$

where $u_{i,j}$ and $P_{i,j}$ are the normalized 10-minute average values of wind speed and power, and N_i is the number of 10-minute data sets in the i^{th} bin. For the power curve to be complete and reliable, each wind speed bin must include at least 30 minutes of sampled data. Furthermore, the total measurement time must cover at least a period of 180 hours. The range of wind speeds must range from 1 m/s below cut-in wind speed to 1.5 times the wind speed at 85% of the rated power of the wind turbine. The IEC power curve can be defined as

$$P_{IEC}(u_i) = P_i\,. \tag{1.41}$$

A typical IEC power curve is presented in Fig. 1.4.

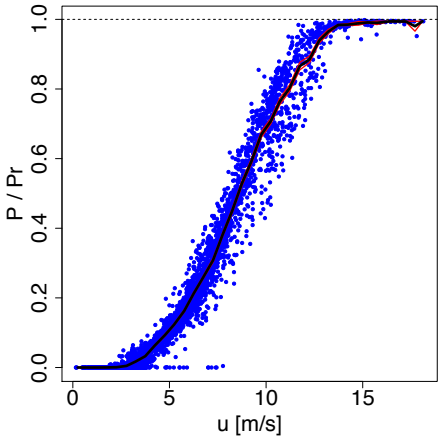

Figure 1.4: IEC power curve $P_{IEC}(u)$ (black line) enclosed in error estimate (enclosing red lines) obtained according to the IEC norm. The 10-minute averages are shown in the background (blue dots).

1.3.4 Estimation of Annual Energy Production

The IEC norm [109] also defines the AEP (Annual Energy Production) and a method of estimation. The AEP is a central feature for economical considerations, as it gives a first estimate of the long-time energy production of a wind turbine (see Ref. [112] for a detailed survey on wind energy economics). The estimation of the AEP extrapolates the power production of a wind turbine characterized by its power curve in a given location.

Any location scheduled to host a wind turbine can be categorized in advance by a characterization of its wind resource. A local measurement of wind speed u from a met mast at hub height[j] of the hypothetical wind turbine must be performed, typically over one year[k]. The

[j] If a measurement at hub height $z \sim 100$m is unavailable due to technical difficulties, a vertical extrapolation can be performed from measurements at lower heights.

[k] A measurement of wind speed over one year covers the various wind situations resulting from various seasonal behaviors.

probability density function $f(u)$ of the ten-minute average values of u is established. For long enough measurements, $f(u)$ is known to approach a Weibull distribution [24]

$$f_W(u;k,c) = \frac{k}{c}\left(\frac{u}{c}\right)^{k-1} e^{(-u/c)^k}, \tag{1.42}$$

where k and c are called respectively the shape and scale factors[l], see Ref. [1] for some examples.

While $f(u) \simeq f_W(u;k,c)$ characterizes a given location, a wind turbine is (approximately) characterized by its IEC power curve, that serves as an average transfer function from wind speed u to power output P. An estimation of the average power output $\langle P \rangle$ can be obtained following

$$\langle P \rangle = \int_0^\infty f_W(u) \times P_{IEC}(u)\, du\,. \tag{1.43}$$

An estimation of the energy production over a period T is $\langle P \rangle \times T$. Over one year, $T = 8760$h and $AEP = \langle P \rangle \times 8760$h where $\langle P \rangle$ and AEP are given resp. in W and Wh.

The AEP can predict how much energy a wind turbine will generate on a given site before installing it. This allows for an optimal choice of design for the optimal location. This result however remains a rough estimation, as it neglects e.g. wake losses generated by other surrounding wind turbines.

1.3.5 Langevin power curve

From a simple mechanical perspective, a wind turbine could be seen as a black box that continually adapts its power output to the ever-changing, turbulent wind speed. One can intuitively postulate that fast wind fluctuations are filtered out by the turbine due to its inertia (that is related to the rotor size and to the control strategy). However, slower changes in wind speed should bring changes in power output. Ref. [113] proposes to describe such dynamics as a relaxation process towards a stationary power curve. Ref. [114] supports this description, and illustrates that the conversion process drifts towards a dynamically attractive power curve that will be named the *Langevin power curve*[m] $P_L(u)$. As the wind speed changes from u_1 to a new value $u_2 \neq u_1$, the power production adapts by drifting slowly[n] from $P_L(u_1)$ towards a new power value $P_L(u_2)$. The relaxation process is illustrated in figure 1.5.

The Langevin power curve is defined as the attractive fixed points of the drift coefficient [114]. It is the deterministic attractor of the stochastic system. For a one-dimensional dynamical system, the drift coefficient is defined as the first Kramers-Moyal coefficient, see equation (1.19). An extension to a two-dimensional system is straightforward, see [41]. Considering the

[l] The IEC norm [109] refers to the Rayleigh distribution, which is a special case of the Weibull distribution for $k = 2$.

[m] In former publications on the topic, the Langevin power curve was called *dynamical power curve* or *Markovian power curve*. It is nonetheless the same approach.

[n] The drift is considered to be slow because it is seen in real data that the wind speed is the fast-changing variable and the power output is the slower variable. In the case $u_1 \to u_2$, wind turbines seldom reach the power value $P_L(u_2)$. Instead, a new wind speed value $u_3 \neq u_2$ arises before $P_L(u_2)$ is reached. The wind turbine continually tries to adapt $P(t)$ to a fast, ever-changing wind speed $u(t)$.

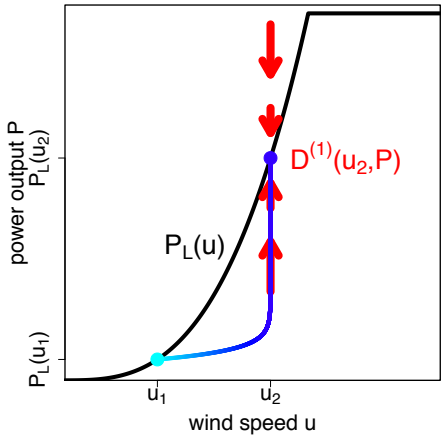

Figure 1.5: Conceptual illustration of the relaxation process for $P(t)$. When the wind speed changes from u_1 to u_2, the power output is slowly driven by the drift field $D^{(1)}(u_2,P)$ (red arrows) from the old stable value $P_L(u_1)$ to a new stable value $P_L(u_2)$ (blue trajectory). The Langevin power curve $P_L(u)$ represents the stable, attractive fixed points of the system.

dynamics of the turbine in the two-dimensional state space $\{u;P\}$, one can define for each local state (u_i,P_j) the drift coefficient $D_u^{(1)}$ in the $u-$direction following

$$D_u^{(1)}(u_i,P_j) = \lim_{\tau\to 0}\frac{1}{\tau}\Big\langle u(t+\tau)-u(t)\Big|u(t)=u_i,P(t)=P_j\Big\rangle\,, \tag{1.44}$$

as well as the drift coefficient $D_P^{(1)}$ in the $P-$direction following

$$D_P^{(1)}(u_i,P_j) = \lim_{\tau\to 0}\frac{1}{\tau}\Big\langle P(t+\tau)-P(t)\Big|u(t)=u_i,P(t)=P_j\Big\rangle\,. \tag{1.45}$$

Considering that the wind speed drives the power output, and not the opposite, the dynamics in the $u-$direction are not a relevant measure of the wind turbine dynamics. The wind speed dynamics $\dot{u}$ are influenced by many external effects which are not in the scope of this work. Instead, the conversion process $u\to P$ is of interest here, and only the reaction of power output to changing wind speed is investigated. This is why in this work, $D_u^{(1)}$ is not used and only $D^{(1)}\equiv D_P^{(1)}$ is considered. That is, only the projection in the $P-$direction is investigated. A representation of a typical drift coefficient can be found in figure 1.6.

The stable, attractive fixed points of $D^{(1)}(u_i,P_j)$ define the Langevin power curve $P_L(u_i)$ following

$$\begin{aligned} D^{(1)}\big(u_i,P_L(u_i)\big) &= 0 \\ \left.\frac{\partial D^{(1)}(u_i,P_j)}{\partial P}\right|_{P_j=P_L(u_i)} &< 0\,. \end{aligned} \tag{1.46}$$

In order to calculate the Langevin power curve, the first step defined in the IEC norm (see section 1.3.3) concerning data measurement and normalization also applies. It should be noted

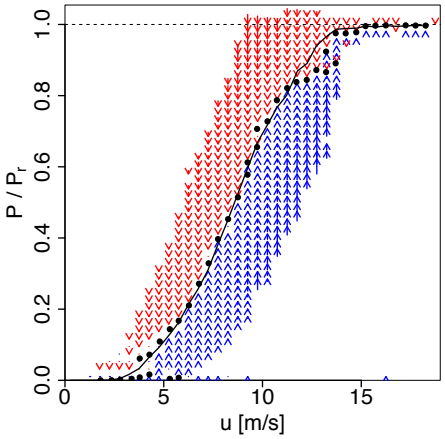

Figure 1.6: Drift function $D^{(1)}(u,P)$ estimated for a multi-MW wind turbine in operation. Each arrow represents the local value of $D^{(1)}(u,P)$ in magnitude (length of the arrow) and direction (pointing up for positive values). The stable fixed points are given by the black dots. The IEC power curve is shown for reference (full line). The rated power P_r is indicated (dashed line).

that for this approach, measuring the wind speed $u(t)$ and power output $P(t)$ at a sampling frequency of at least 1Hz is essential in order to capture the fast conversion dynamics. A comparison of IEC and Langevin power curves is presented in figure 1.6. An estimation of the uncertainty for $P_L(u)$ is proposed in Ref. [115].

One could speak of a state-based averaging in the $\{u,P\}$ space, in contrast to the temporal averaging performed in the IEC norm. The dynamics of the power signal can be directly related to the local sign and value of $D^{(1)}$. A positive drift indicates that the power tends to increase (blue arrows pointing up in figure 1.6), in regions where the wind turbine does not produce enough power for the given wind speed. On the contrary, a negative drift corresponds to a decreasing power (red arrows pointing down), in regions where the wind turbine produces too much power for the given wind speed. At the intersection are the stable fixed points where the power dynamics are in a stable configuration (the average time derivative is zero). The Langevin approach can reveal complex dynamics, including e.g. multiple stable states, see also [114, 116]. Such multi-stable dynamics are typically observed in the regions of transition, around cut-in or rated wind speeds, see figure 1.3. The various control strategies are clearly separated thanks to the two-dimensional, state-based averaging procedure[o].

1.A Appendix 1: Derivation of the Kramers-Moyal expansion

The Kramers-Moyal expansion presented in section 1.2.2 is derived in this appendix. The demonstration presented in this appendix 1.A is done in greater detail in Ref. [41].

[o]The IEC approach averages all the power values for each wind speed bin, such that multi-stable dynamics are filtered out.

The characteristic function C is defined as the Fourier transform of the probability following

$$C(k) = \int_{-\infty}^{\infty} e^{ikx} f(x) dx . \tag{1.47}$$

A characteristic function can be defined similarly for a conditional probability following

$$\begin{aligned} C(k,x',t,\tau) &= \int_{-\infty}^{\infty} dx\, e^{ik(x-x')} p(x,t+\tau|x',t) \\ &= \int_{-\infty}^{\infty} dx \sum_{n=0}^{\infty} \frac{[ik(x-x')]^n}{n!} p(x,t+\tau|x',t) \\ &= \sum_{n=0}^{\infty} \frac{(ik)^n}{n!} \int_{-\infty}^{\infty} dx\, (x-x')^n p(x,t+\tau|x',t) \\ &= \sum_{n=0}^{\infty} \frac{(ik)^n}{n!} M^{(n)}(x',t,\tau) \\ &= 1 + \sum_{n=1}^{\infty} \frac{(ik)^n}{n!} M^{(n)}(x',t,\tau) . \end{aligned} \tag{1.48}$$

The conditional moments $M^{(n)}$ are defined in equation (1.17). Also, $M^{(0)}(x',t,\tau) = 1$ is used.

The opposite relation gives the conditional probability as the inverse Fourier transform of the characteristic function

$$\begin{aligned} p(x,t+\tau|x',t) &= \frac{1}{2\pi} \int_{-\infty}^{\infty} dk\, e^{-ik(x-x')} C(k,x',t,\tau) \\ &= \frac{1}{2\pi} \int_{-\infty}^{\infty} dk\, e^{-ik(x-x')} \left[1 + \sum_{n=1}^{\infty} \frac{(ik)^n}{n!} M^{(n)}(x',t,\tau) \right] \end{aligned} \tag{1.49}$$

using equation (1.48). Using the property of the delta function

$$\delta(x-x') = \frac{1}{2\pi} \int_{-\infty}^{\infty} dk\, e^{-ik(x-x')} \tag{1.50}$$

and differentiating it n-times (with $n \geq 0$) gives

$$\left(-\frac{\partial}{\partial x} \right)^n \delta(x-x') = \frac{1}{2\pi} \int_{-\infty}^{\infty} dk\, (ik)^n e^{-ik(x-x')} . \tag{1.51}$$

One can reformulate equation (1.49) using equations (1.50,1.51) and

$$\begin{aligned} p(x,t+\tau|x',t) &= \frac{1}{2\pi} \int_{-\infty}^{\infty} dk\, e^{-ik(x-x')} \\ &\quad + \sum_{n=1}^{\infty} \frac{1}{n!} \frac{1}{2\pi} \int_{-\infty}^{\infty} dk\, (ik)^n e^{-ik(x-x')} M^{(n)}(x',t,\tau) \\ &= \delta(x-x') + \sum_{n=1}^{\infty} \frac{1}{n!} \left(-\frac{\partial}{\partial x} \right)^n M^{(n)}(x',t,\tau) \delta(x-x') \\ &= \left[1 + \sum_{n=1}^{\infty} \frac{1}{n!} \left(-\frac{\partial}{\partial x} \right)^n M^{(n)}(x',t,\tau) \right] \delta(x-x') . \end{aligned} \tag{1.52}$$

Inserting equation (1.52) into equation (1.16) gives

$$f(x,t+\tau) = \int dx' \left[1 + \sum_{n=1}^{\infty} \frac{1}{n!} \left(-\frac{\partial}{\partial x} \right)^n M^{(n)}(x',t,\tau) \right] \delta(x-x') f(x',t)$$
$$= \left[1 + \sum_{n=1}^{\infty} \frac{1}{n!} \left(-\frac{\partial}{\partial x} \right)^n M^{(n)}(x,t,\tau) \right] f(x,t) \,. \tag{1.53}$$

One can derive the Kramers-Moyal expansion

$$\begin{aligned} \frac{\partial f(x,t)}{\partial t} &= \lim_{\tau \to 0} \frac{f(x,t+\tau) - f(x,t)}{\tau} \\ &= \lim_{\tau \to 0} \frac{1}{\tau} \sum_{n=1}^{\infty} \frac{1}{n!} \left(-\frac{\partial}{\partial x} \right)^n M^{(n)}(x,t,\tau) f(x,t) \\ &= \sum_{n=1}^{\infty} \left(-\frac{\partial}{\partial x} \right)^n \frac{1}{n!} \lim_{\tau \to 0} \frac{1}{\tau} M^{(n)}(x,t,\tau) f(x,t) \\ &= \sum_{n=1}^{\infty} \left(-\frac{\partial}{\partial x} \right)^n D^{(n)}(x,t) f(x,t) \end{aligned} \tag{1.54}$$

with the Kramers-Moyal coefficients defined as

$$\begin{aligned} D^{(n)}(x,t) &= \frac{1}{n!} \lim_{\tau \to 0} \frac{1}{\tau} M^{(n)}(x,t,\tau) \\ &= \frac{1}{n!} \lim_{\tau \to 0} \frac{1}{\tau} \Big\langle \big[x(t+\tau) - x(t) \big]^n \Big| x(t) = x \Big\rangle \,. \end{aligned} \tag{1.55}$$

It should be noted that in the special case of the Fokker-Planck equation ($D^{(n)} = 0$ for $n > 2$), the short-time propagator $p(x,t+\tau|x',t)$ can be simplified. Based on the definition of $\delta(x-x')$ in equation (1.50), equation (1.28) becomes for small time increments τ

$$\begin{aligned} p(x,t+\tau|x',t) &= e^{\tau L_{FP}(x,t)} \delta(x-x') \\ &= exp \left[-\tau \frac{\partial}{\partial x} D^{(1)}(x',t) + \tau \frac{\partial^2}{\partial x^2} D^{(2)}(x',t) \right] \frac{1}{2\pi} \int_{-\infty}^{\infty} dk \, e^{ik(x-x')} \\ &= \frac{1}{2\pi} \int_{-\infty}^{\infty} dk \, exp \left[-\tau D^{(1)}(x',t) \frac{\partial}{\partial x} + \tau D^{(2)}(x',t) \frac{\partial^2}{\partial x^2} \right] e^{ik(x-x')} \\ &= \frac{1}{2\pi} \int_{-\infty}^{\infty} dk \, exp \Big[-\tau D^{(1)}(x',t) ik - \tau D^{(2)}(x',t) k^2 + ik(x-x') \Big] \\ &= \frac{1}{\sqrt{4\pi\tau D^{(2)}(x',t)}} exp \left(-\frac{[x-x'-\tau D^{(1)}(x',t)]^2}{4\tau D^{(2)}(x',t)} \right) \end{aligned} \tag{1.56}$$

using the identity $\int_{-\infty}^{\infty} e^{-ax^2+bx} dx = \sqrt{\frac{\pi}{a}} \, e^{b^2/4a}$ for $a > 0$.

1.B Appendix 2: Connection of the Langevin equation with the Fokker-Planck equation

The Langevin equation is introduced in equation (1.31) with the Kramers-Moyal coefficients previously defined in equation (1.19). This connects the Fokker-Planck and Langevin equations, that describe the same stochastic properties. Yet this connection is not obvious, and it is the purpose of this appendix to demonstrate it.

Based on the structure of the stochastic equation (1.3) introduced by Langevin, the general form of the Langevin equation for a one-dimensional Langevin process $x(t)$ is

$$\frac{dx}{dt} = h(x,t) + g(x,t)\cdot\Gamma(t)\,. \tag{1.57}$$

The Langevin noise (also called Langevin *force*) $\Gamma(t)$ is a Gaussian distributed, uncorrelated (white) noise that follows $\langle\Gamma(t)\rangle = 0$ and $\langle\Gamma(t)\Gamma(t')\rangle = 2\delta(t-t')$.

From the identity

$$\begin{aligned} x(t+\tau) - x(t) &= \int_t^{t+\tau} dt'\ \frac{dx}{dt}(t') \\ &= \int_t^{t+\tau} dt'\ \Big[h(x,t') + g(x,t')\cdot\Gamma(t')\Big] \end{aligned} \tag{1.58}$$

one can derive

$$\begin{aligned} D^{(1)}(x_0,t) &= \lim_{\tau\to 0}\frac{1}{\tau}\Big\langle x(t+\tau) - x(t)\Big| x(t) = x_0\Big\rangle \\ &= \lim_{\tau\to 0}\frac{1}{\tau}\left\langle \int_t^{t+\tau} dt'\ \Big[h(x,t') + g(x,t')\cdot\Gamma(t')\Big]\right| x(t) = x_0\Bigg\rangle \\ &= \lim_{\tau\to 0}\frac{1}{\tau}\left\langle \left[h(x,t)\int_t^{t+\tau} dt' + g(x,t')\int_t^{t+\tau} dt'\,\Gamma(t')\right]\right| x(t) = x_0\Bigg\rangle \\ &= h(x_0,t) + g(x_0,t)\lim_{\tau\to 0}\frac{1}{\tau}\int_t^{t+\tau} dt'\Big\langle\Gamma(t')\Big| x(t) = x_0\Big\rangle \\ &= h(x_0,t)\,. \end{aligned} \tag{1.59}$$

considering $\int_t^{t+\tau} h(x,t')dt' = h(x,t)\tau$ for the vanishing time duration τ. Similarly, g was taken out of the integral following Itô definition of stochastic integrals, see equation (1.33). The identity

$\langle \Gamma(t')|x(t)=x_0\rangle = 0$ follows the definition of Γ. Also,

$$\begin{aligned}
D^{(2)}(x_0,t) &= \frac{1}{2}\lim_{\tau\to 0}\frac{1}{\tau}\left\langle \Big[x(t+\tau)-x(t)\Big]^2 \middle| x(t)=x_0 \right\rangle \\
&= \frac{1}{2}\lim_{\tau\to 0}\frac{1}{\tau}\left\langle \int_t^{t+\tau} dt' \Big[h(x,t')+g(x,t')\cdot\Gamma(t')\Big] \right. \\
&\qquad \left. \int_t^{t+\tau} dt'' \Big[h(x,t'')+g(x,t'')\cdot\Gamma(t'')\Big] \middle| x(t)=x_0 \right\rangle \\
&= \frac{1}{2}\lim_{\tau\to 0}\frac{1}{\tau}\left\langle \int_t^{t+\tau}\int_t^{t+\tau} dt'dt''\, h(x,t')h(x,t'') \right. \\
&\qquad \left. + \int_t^{t+\tau}\int_t^{t+\tau} dt'dt''\, g(x,t')\Gamma(t')g(x,t'')\Gamma(t'') \middle| x(t)=x_0 \right\rangle \\
&= \frac{1}{2}\Big[h(x,t_0)\Big]^2 \lim_{\tau\to 0}\tau \\
&\qquad + \frac{1}{2}\Big[g(x,t_0)\Big]^2 \lim_{\tau\to 0}\frac{1}{\tau}\int_t^{t+\tau}\int_t^{t+\tau} dt'dt'' \left\langle \Gamma(t')\Gamma(t'') \middle| x(t)=x_0 \right\rangle \\
&= \frac{1}{2}\Big[g(x,t_0)\Big]^2 \lim_{\tau\to 0}\frac{1}{\tau}\int_t^{t+\tau}\int_t^{t+\tau} dt'dt''\, 2\delta(t'-t'') \\
&= \Big[g(x,t_0)\Big]^2 . \qquad (1.60)
\end{aligned}$$

Injecting equations (1.59,1.60) into the generalized Langevin equation (1.57) yields the common form

$$\frac{dx}{dt} = D^{(1)}(x,t) + \sqrt{D^{(2)}(x,t)}\cdot\Gamma(t)\,. \qquad (1.61)$$

1.C Appendix 3: Aerodynamics of rotor blades[a]

The essential (mechanical) element of a wind turbine is the rotor, that transforms the power of the wind into a rotational or mechanical power. The ideal requirements are:

- the rotation should be steady and smooth;
- dynamical loads should be minimal;
- the regulation should be done without sudden jumps.

[a]This section is a summary of a book chapter that has been accepted, and is being published as PATRICK MILAN, MATTHIAS WÄCHTER and JOACHIM PEINKE: Wind Turbine Power Performance and Application to Monitoring, in *Handbook of Wind Power Systems (HWPS): Optimization, Modeling, Simulation and Economic Aspects*, editors S. Rebennack, P. M. Pardalos, V. Pappu, M. V. Pereira and N. A. Illiadis, publisher Springer, 2013.

The number of blades, their profile and design should guarantee these features. Modern wind turbines rotate due to the lift forces F_L acting on the airfoils. For an airfoil the effective area can be expressed in terms of the depth t and the wingspan b (similar to the rotor radius R), such that

$$\begin{aligned} F_D &= C_D(\alpha)\frac{1}{2}\rho c^2(t\cdot b) \\ F_L &= C_L(\alpha)\frac{1}{2}\rho c^2(t\cdot b)\,, \end{aligned} \tag{1.62}$$

where α is the angle of attack, as displayed in figure 1.7. The lift-to-drag ratio F_L/F_D relates to the quality of the airfoil, which should be maximized.

In figure 1.7, the velocity vector $\mathbf{c}$ gives the wind velocity in the frame of reference of the airfoil. The wind velocity at the rotor is $\frac{2}{3}\mathbf{u}$ in the frame of the ground, where u is the wind velocity upstream, see section 1.3.1. Additionally, the rotational motion must be considered for the motion of the wind with respect to the blades. The velocity of the rotational motion at a radial position r is $v=\omega r$, such that

$$c^2(r) = (2u/3)^2 + (\omega r)^2 \tag{1.63}$$

gives the effective velocity c of the air in the reference frame of the blade, see figure 1.7.

Blade element momentum theory is commonly used to estimate the total force acting on the rotor by summing up the local force on each infinitesimal blade element of size dr. The total force is divided into its rotational component F_r and its axial component F_a. Considering an infinitesimal cut dr at radial position r in the polar plane of the rotor, the infinitesimal components are

$$\begin{aligned} dF_r &= \frac{\rho}{2}c^2\cdot t\cdot dr\Big[C_L cos(\gamma) - C_D sin(\gamma)\Big] \\ dF_a &= \frac{\rho}{2}c^2\cdot t\cdot dr\Big[C_L sin(\gamma) + C_D cos(\gamma)\Big]\,. \end{aligned} \tag{1.64}$$

The angle $\gamma = \frac{\pi}{2} - \alpha - \beta$ (see figure 1.7) reads

$$tan(\gamma) = \frac{\omega r}{2u/3} = \frac{3}{2}\frac{\omega R}{u}\frac{r}{R} = \frac{3}{2}\lambda\frac{r}{R}\,. \tag{1.65}$$

Only the rotational component F_r is of use to rotate the rotor[a]. The infinitesimal power associated to the rotational force acting on z rotor blades is

$$\begin{aligned} dP &= z\cdot dF_r\cdot \omega r \\ &= z\cdot\frac{\rho}{2}c^2\cdot t\cdot\omega\cdot r\,dr\Big[C_L cos(\gamma) - C_D sin(\gamma)\Big]\,. \end{aligned} \tag{1.66}$$

The goal is to construct the blades in such a way that they extract the optimal power following Betz limit out of the wind. It should be noted that in this idealized case, the drag force must be

[a]The force F_a in the axial direction does not contribute to the power production but to the thrust acting on the turbine structure. F_a should be minimized to reduce mechanical fatigue.

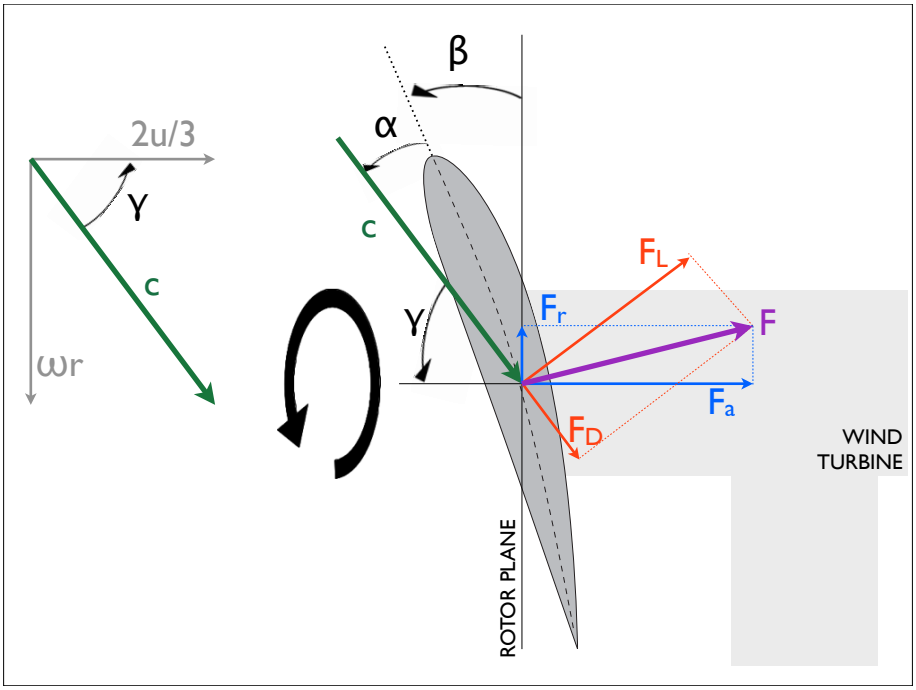

Figure 1.7: Cut through an airfoil rotating around the wind turbine axis. The rotational velocity ωr (gray) is perpendicular to the axial velocity $2u/3$ (gray). The angle of attack α is the angle between the air velocity $\mathbf{c}$ (green) and airfoil chord (dashed line). The pitch angle β denotes the angle between the chord and the plane of rotation. The lift and drag forces F_L and F_D are displayed (red), giving the total force F (purple), as well as the rotational and thrust projections F_r and F_a (blue).

zero, which can be practically approached if $C_D \ll C_L$. Each infinitesimal radial annulus of size $2\pi r dr$ should extract a fraction $16/27$ of the wind power

$$\begin{aligned} dP_{ideal} &= \frac{16}{27} \cdot \frac{\rho}{2} \cdot u^3 \cdot (2\pi r dr) \\ &= z\frac{\rho}{2} c^2 \cdot t \cdot \omega \cdot r dr \cdot C_L cos(\gamma) \end{aligned} \tag{1.67}$$

based on equation (1.66). In order to approach such ideal case, the blade depth $t(r)$ must follow

$$t(r) = \frac{16\pi}{9} \cdot \frac{R^2}{zC_L\lambda^2} \cdot \frac{\omega}{c} \approx \frac{16\pi}{9} \frac{R^2}{zC_L r\lambda^2}, \tag{1.68}$$

where the approximation holds for high rotational speed $\omega \gg u/r$, and $c \approx \omega r$. This approximation is valid away from the blade root and for fast-rotating turbines. This has an important consequence on the design of rotor blades. The depth decreases when increasing either the number of blades, the lift coefficient, the radius or the tip speed ratio. This explains why fast rotating wind turbines tend to have only two or three narrow blades to optimize power extraction, while old western-mill machines have many, rather broad blades (in order to maximize mechanical torque).

If drag losses are included, an efficiency factor η_{drag} can be introduced as the ratio of real to ideal power

$$\begin{aligned}\eta_{drag} = \frac{dP}{dP_{ideal}} &= \frac{C_L cos(\gamma) - C_D sin(\gamma)}{C_L cos(\gamma)} \\ &= 1 - \frac{C_D}{C_L} tan(\gamma) \\ &= 1 - \frac{C_D}{C_L} \frac{3}{2R} \lambda r \end{aligned} \tag{1.69}$$

following equation (1.65). This justifies the large profile losses for large tip speed ratios in figure 1.2.

Bibliography

[1] T. Burton, D. Sharpe, N. Jenkins, and E. Bossanyi. *Wind energy handbook*. Wiley, New York, 2001.

[2] I Marusic, BJ McKeon, PA Monkewitz, HM Nagib, AJ Smits, and KR Sreenivasan. Wall-bounded turbulent flows at high reynolds numbers: Recent advances and key issues. *Physics of Fluids*, 22:065103, 2010.

[3] Allan Morales, Matthias Wächter, and Joachim Peinke. Characterization of wind turbulence by higher-order statistics. *Wind Energy*, 15:391–406, 2012.

[4] Frank Böttcher, Stephan Barth, and Joachim Peinke. Small and large fluctuations in atmospheric wind speeds. *Stoch Environ Res Ris Assess*, 21:299–308, 2007.

[5] Isaac Van der Hoven. Power spectrum of horizontal wind speed in the frequency range from 0.0007 to 900 cylcles per hour. *Journal of Meteorology*, 14(2):160–164, 1957.

[6] R I Harris. The macrometeorological spectrum - a preliminary study. *Journal of Wind Engineering and Industrial Aerodynamics*, 96(12):2294–2307, 12 2008.

[7] U. Frisch. Turbulence. The legacy of of A. N. Kolmogorov. *Cambridge University Press*, 1995.

[8] R Friedrich, M Voßkuhle, O Kamps, and M Wilczek. Two-point vorticity statistics in the inverse turbulent cascade. *arXiv preprint arXiv:1012.3356*, 2010.

[9] F. Schmitt, D. Schertzer, S. Lovejoy, and Y. Brunet. Estimation of universal multifractal indices for atmospheric turbulent velocity fields. *Fractals*, 102(3):568–575, 1993.

[10] S. Lovejoy, D. Schertzer, and J. D. Stanway. Direct evidence of multifractal atmospheric cascades from planetary scales down to 1 km. *Phys. Rev. Lett.*, 86(22):5200–5203, 2001.

[11] S. Lovejoy, D. Schertzer, V. Allaire, T. Bourgeois, S. King, J. Pinel, and J. Stolle. Atmospheric complexity or scale by scale simplicity? *Geophysical Research Letters*, 36(1), 2009.

3.4 Exercise

Exercise 3.1 ***Study of a time series of a Turbulent Flow***

In this Exercise, you will analyze with Mathematica a time series of a Turbulent Flow, an air into air round free jet. The corresponding Experiment, which uses Hot Wire Anemometry, has been described in Renner *et al.* (2001).
The time series is available on the web page of the module, under the link

http://emmanuelplaut.perso.univ-lorraine.fr/afm/Jet.dat .

The file `Jet.dat` contains velocity measurements $u(t)$ in m/s with a sampling frequency of 8 kHz, i.e., $t = t_n = nT$ with $n \in \{1, \cdots, N_d\}$ and $T = 1/(8\text{ kHz})$.

1 Import the file `Jet.dat`, compute the number N_d of data points, and plot the whole time series.
Indication: the command `Flatten` will help to get a list of numbers, not a list of lists.

2 Prepare two lists where you take either the first 5000 or the last 5000 data points. Plot the time series of the first 5000 and the last 5000 data points. Compare and comment.

3 Determine the mean velocity $\langle u(t) \rangle_t$ for the first 5000 and for the last 5000 data points. Compare and comment.

4.a Construct a list with the histogram of the data $u(t)$, normalized as a Probability Density Function, and plot it. Comment.
Indications:
Your code should have the following structure, to produce a list with u at the first place and $p(u)$ at the second place:

```
h= HistogramList[..., Automatic, "PDF"]

hup= {};
Do[AppendTo[hup,{(h[[1,n+1]]+h[[1,n]])/2,h[[2,n]]}], {n,Length[h[[2]]]}]

ListPlot[hup, ...]
```

4.b Plot the PDF of u but in linear - log scales. Comment on the character, Gaussian or non Gaussian, of $u(t)$.

5.a Construct a list with the velocity increments

$$u_\tau(t_n) \;=\; u(t_n + \tau) - u(t_n) \;,$$

for $\tau = 10T$, i.e.

$$u_\tau(t_n) \;=\; u(t_{n+10}) - u(t_n) \;.$$

Plot this time series, that we denote hereafter $u_{10}(t)$.

5.b Plot the time series of the first 5000 data points $u_{10}(t)$. Compare with the plots of question 2 and comment.

5.c Do what you did for u in questions 4 but for u_{10}: construct a list with the histogram of the data $u_{10}(t)$, normalized as a Probability Density Function, and plot it; comment; plot this PDF of u_{10} but in linear - log scales; comment on the character, Gaussian or non Gaussian, of $u_{10}(t)$.

Bibliography

Bodenschatz, E., Pesch, W. & Ahlers, G. 2000 Recent developments in Rayleigh-Bénard Convection. *Annu. Rev. Fluid Mech.* **32**, 709–778.

Busse, F. H. 2003 The sequence-of-bifurcations approach towards understanding turbulent fluid flow. *Surveys in Geophys.* **24**, 269–288.

Castaing, B., Gagne, Y. & Hopfinger, E. 1990 Velocity probability density functions of high Reynolds number turbulence. *Physica D* **46**, 177–200.

Davis, G. D. V. 1983 Natural convection of air in a square cavity: a benchmark numerical solution. *Int. J. Numer. Methods Fluids* **3**, 249.

Friedrich, R. & Peinke, J. 2009 Fluid Dynamics, Turbulence. *Encyclopedia of Complexity and Systems Science* (ed. R. A. Meyers), pp. 3641–3661. Springer New York, DOI: 10.1007/978-0-387-30440-3_215.

Frisch, U. 1995 *Turbulence. The legacy of Kolmogorov*. Cambridge University Press.

Haken, H. 1983 *Synergetics - An introduction*. Springer-Verlag.

Hu, Y., Ecke, R. & Ahlers, G. 1993 Convection near threshold for Prandtl numbers near 1. *Phys. Rev. E* **48**, 4399–4413.

Jenny, M. 2014 *Machines à fluides - Turbomachines*. Cours de l'école des Mines de Nancy (2A), http://energie.mines-nancy.univ-lorraine.fr/2A/turbo2a.pdf.

Milan, P., Wächter, M. & Peinke, J. 2013 Turbulent Character of Wind Energy. *Phys. Rev. Lett.* **110**, 138701, DOI: 10.1103/PhysRevLett.110.138701.

Naert, A., Castaing, B., Chabaud, B., Hebral, B. & Peinke, J. 1998 Conditional statistics of velocity fluctuations in turbulence. *Physica D* **113**, 73–78.

Plapp, B. B. 1997 Spiral pattern formation in Rayleigh-Benard convection. PhD thesis, Cornell University.

Plaut, E. 2008 *Modélisation d'instabilités : méthodes non linéaires*. Cours du Master 2 recherche de mécanique-énergétique de Nancy, téléchargeable sur http://emmanuelplaut.perso.univ-lorraine.fr/publisp.

Plaut, E. 2014 *Mécanique des fluides*. Cours de l'école des Mines de Nancy (2A), http://emmanuelplaut.perso.univ-lorraine.fr/mf/pol.pdf.

Renner, C., Peinke, J. & Friedrich, R. 2001 Experimental indications for Markov properties of small-scale turbulence. *J. Fluid Mech.* **433**, 383–409, DOI: 10.1017/S0022112001003597.

Reynolds, O. 1895 On the dynamical theory of incompressible viscous fluids and the determination of the criterion. *Phil. Trans. Roy. Soc. Lond.* **186**, 123–164.

Stasiek, J. 1997 Thermochromic liquid crystals and true colour image processing in heat transfer and fluid-flow research. *Heat and Mass Transfer* **33**, 27–39.

Stresing, R. & Peinke, J. 2010 Towards a stochastic multi-point description of turbulence. *New J. Phys.* **12**, 103046, DOI: 10.1088/1367-2630/12/10/103046.

Wächter, M., Heisselmann, H., Hölling, M., Morales, A., Milan, P., Mücke, T., Peinke, J., Reinke, N. & Rinn, P. 2012 The turbulent nature of the atmospheric boundary layer and its impact on the wind energy conversion process. *J. Turb.* **13**, N26, DOI: 10.1080/14685248.2012.696118.